ELSEVIER

Contents lists available at ScienceDirect

Journal of Membrane Science

journal homepage: www.elsevier.com/locate/memsci





Effect of the annealing temperature of polybenzimidazole membranes in high pressure and high temperature H₂/CO₂ gas separations

Edson V. Perez*, John P. Ferraris, Kenneth J. Balkus Jr., Inga H. Musselman

Department of Chemistry and Biochemistry, The University of Texas at Dallas, Richardson, TX, 75080, USA

ARTICLE INFO

Keywords: High temperature/high pressure H₂/CO₂ gas mixture separation Polybenzimidazole membrane High temperature annealing Activation energy of permeation

ABSTRACT

The effect of the annealing temperature of polybenzimidazole (PBI) membranes on H₂/CO₂ gas separations was investigated. Membranes annealed from 250 °C to 400 °C were tested for gas permeation with pure H2, CO2, and N_2 gases and a H_2 : CO_2 (1:1) mixture at 35 °C, 100 °C, 200 °C, and 300 °C and at pressures up to 45 bar. Gas permeation data show that permeability and selectivity of the membranes is significantly impacted by the annealing temperature, the presence of adsorbed water, and remaining casting solvent (DMAc). At a testing temperature of 35 °C, ideal H₂/CO₂ selectivities of 50, 49, and 66 with pure H₂ permeabilities of 1.5, 0.8, and 1.5 Barrer were obtained for membranes annealed at 250 °C, 300 °C, and 400 °C, respectively. At this temperature, high gas mixture H₂/CO₂ selectivities of 41, 73, and 47 with H₂ permeabilities of 1.03, 0.26, and 0.50 Barrer were also obtained for these membranes. At testing temperatures of 300 °C, both the ideal and gas mixture H₂/ CO_2 selectivities dropped to 44, 28, and 30 (ideal, $H_2=45$, 45, 44 Barrer) and to 19, 22, and 23 (mixture, $H_2=45$, 45, 45, 44 Barrer) and to 19, 22, and 23 (mixture, $H_2=45$, 45, 45, 47, 48 Barrer) and $H_2=45$, 47, 48 Barrer) and $H_2=45$, 48, 49, 41 Barrer) and $H_2=45$, 48, 49, 41 Barrer) and $H_2=45$, 42 Barrer) and $H_2=45$, 41 Barrer) and $H_2=45$, 42 Barrer) and $H_2=45$, 41 Barrer) and $H_2=45$, 42 Barrer) and $H_2=45$, 43 Barrer) and $H_2=45$, 45 Barrer) and $H_2=45$, 47 Barrer) and $H_2=45$, 48 Barrer) and $H_$ 41, 43, and 44 Barrer) for membranes annealed at 250 °C, 300 °C, and 400 °C, respectively. As water was removed from the membranes at temperatures greater than 100 °C during permeation cycles, where the testing temperature was increased from 35 °C to 300 °C, the permselectivity properties of the membranes annealed at 400 °C became more reproducible. Permeabilities at 35 °C from a second permeability cycle increased, but H₂/ CO_2 selectivities decreased to 21 for gas mixtures ($H_2 = 1.4$ Barrer) and to 34 for pure gases ($H_2 = 2.2$ Barrer). The results suggest that high annealing temperatures may induce changes in the configuration and conformation of the polymer chains, imparting distinctive permselectivity properties to the membranes. Activation energies of permeability for H2, CO2, and N2 from pure gases and H2:CO2 mixtures correlated with these changes as well.

1. Introduction

It is projected that the demand for energy will increase by as much as 56% by 2040 with fossil fuels continuing to provide much of the energy until new sources of energy replace them [1,2]. The utilization of fossil fuels ensures a long-term and low-cost energy supply either as fuel for the generation of electricity in coal plants or as feedstock for the production of hydrogen [3]. In either case, the utilization of fossil fuels will inevitably result in the production of carbon dioxide, a greenhouse gas implicated in climate change. For the clean production of hydrogen, carbon dioxide would need to be removed from the $H_2/CO_2/CO$ mixture produced from the gasification or methane reforming processes of fossil fuels [2,4] and from the water-gas shift reaction (WGSR) that converts carbon monoxide and water into hydrogen and carbon dioxide. The WGSR is an important reaction not only for the production of fuels but also for the Haber-Bosch process in the production of ammonia from

hydrogen and nitrogen [5,6], which is carried out using hydrogen produced in the WGSR [7].

For efficient and clean production of hydrogen, it is desirable that the separation and capture of carbon dioxide be performed at temperatures and pressures similar to WGSR conditions. Research to address this problem has been focused on the fabrication of new inorganic and polymer-based membrane materials for the purification of hydrogen from carbon dioxide in the WGSR [8–12]. A membrane capable of efficiently separating hydrogen from carbon dioxide *in situ* at low cost is more advantageous than other separation methods (e.g., amine-based carbon dioxide separation) since it requires less energy to operate. The current demands for *in situ* hydrogen separation in the WGSR require a temperature higher than 250 °C [13,14] and a hydrogen partial pressure greater than 7 bar in a H₂/CO₂ blend with a pressure of up to 27 bar [15]. Therefore, testing the performance and mechanical stability of membranes under such pressure and temperature conditions is a

E-mail address: Edson.Perez@utdallas.edu (E.V. Perez).

^{*} Corresponding author.

requirement for the screening of membranes for this application.

Polybenzimidazole membranes (poly 2,2'-(m-phenylene)-5,5′-bibenzimidazole or PBI, Fig. 1) are dense as well as mechanically, thermally, and chemically resilient, which makes them suitable for gas separations at high pressure and high temperature ($\rho=1.28-1.37~g/cm^3$ [16,17], modulus = 6 GPa, $T_g=416$ °C, $T_d=512-600$ °C [16,18], inert to carbon monoxide and to hydrogen sulfide). PBI has been extensively studied for proton exchange membranes in fuel cell applications [19–21], and recently, as a polymer membrane [16–18,22–34] (Table S1 in supporting information) and polymer matrix in mixed-matrix membranes [25,35,36] for gas separations. Selectivities for H_2/CO_2 that range from 3.7 to 20 have been reported for PBI membranes measured at temperatures up to 250 °C [22], which illustrates the difficulty in reproducing its permselectivity properties. Table S1 also shows the wide temperature range of 50 °C–250 °C used for the thermal treatment of the membranes, which could affect their permeation properties.

The wide range of permselectivity properties (e.g., H₂/CO₂ from 3.0 to 55.7) shown in Table S1 is coupled to the various parameters associated with the preparation (e.g., casting solvent, annealing temperature) and testing conditions of the membranes (e.g., pressure, temperature, feed composition, membrane history). This complicates the determination of the true permeability of gases in PBI and the interpretation of permeability results, and is even more problematic for mixed-matrix membranes (MMMs) of PBI because improvements in membrane performance would have to be measured against the properties of the pure polymer. Among the potential parameters affecting the properties of PBI membranes, the effects of annealing temperature and testing conditions on the gas permeation properties were investigated in this work. For this purpose, four sets of PBI membranes containing LiCl were cast from N,N-dimethylacetamide (DMAc) and then subjected to a final annealing temperature of 250 °C, 300 °C, 350 °C, or 400 °C. Permeability experiments with pure H2, CO2, N2, and mixed gases (H2: $\mathrm{CO}_2 = 1:1$) were conducted at temperatures that ranged from 35 °C to 300 $^{\circ}$ C with pressures from 5 to 45 bar to simulate real world conditions on membranes annealed at 250 $^{\circ}$ C, 300 $^{\circ}$ C, and 400 $^{\circ}$ C.

2. Experimental

2.1. Materials

Molecular sieves 4A were purchased from Aldrich and activated at 400 °C and atmospheric pressure for 1 d before use. DMAc was purchased from Fisher Scientific and dried over activated molecular sieves 4A for 1 d before use. PBI powder and a 26 wt% PBI solution in DMAc with 1.5 wt% LiCl were obtained from PBI Performance Products, Inc. Mylar® sheets (25 μm thick) were obtained from Active Industries and used as provisional substrates for membrane casting. Grafoil® graphite sheets 0.5 mm thick were obtained from Lamons and cut to fit the permeation cell and the area of the membrane exposed to gases. For gas permeation experiments, hydrogen, carbon dioxide, and nitrogen gases (>99.999%) and the $H_2\text{:}CO_2=1\text{:}1$ mixture were purchased from Airgas.

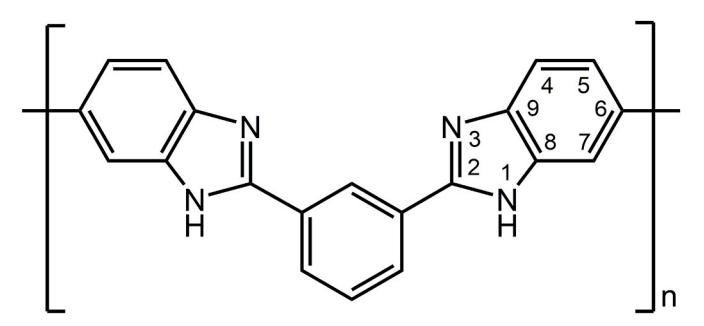


Fig. 1. Structure of PBI.

2.2. Instrumentation and methods

X-ray diffraction (XRD) patterns were acquired from 3° to 45° (20°) at 1°/min using a Rigaku Ultima IV diffractometer with Cu K_{α} ($\lambda=0.154$ nm) X-ray radiation. Fourier transform infrared (FT-IR) spectra of PBI films of thicknesses from 6 μm to 15 μm were recorded with a Nicolet 360 FT-IR spectrometer at room temperature in the range of 400 cm $^{-1}$ to 4000 cm $^{-1}$. Thermogravimetric analyses (TGA) were performed under nitrogen at a heating rate of 5 °C/min from 30 °C to 900 °C using a Mettler Toledo STARe TGA-1 thermogravimetric analyzer. The samples, strips cut from membranes weighing 30 mg–50 mg, were rolled to load enough material into an alumina pan. Scanning electron microscopy (SEM) images were acquired using a LEO Gemini 1500 series microscope and a Zeiss Supra-40 FEI-SEM, both operated at 10 keV. Prior to imaging membrane cross-sections, freeze-fractured membranes were mounted on carbon tape and coated with Au/Pd using a Denton Vacuum Desk II sputter coater.

Mass spectra of a membrane annealed at 250 °C was obtained at the University of Michigan using a Waters Autospec Ultima magnetic sector mass spectrometer. The spectrometer was run in the electron impact ionization mode at 70 eV with the ion source heated to 240 °C. The mass spectrometer was scanned from m/z 10 to m/z 150 every 1.5 s while a sample of the membrane, loaded in a capillary tube, was heated under vacuum from 150 °C to 450 °C according to the following temperature program: heat from room temperature to 150 °C to desorb adsorbed water, hold at 150 °C for 15 min, ramp from 150 °C to 300 °C at 25 °C/min, ramp from 300 °C to 450 °C at 5 °C/min, and hold at 450 °C for 30 min

Single gas and gas mixture permeation measurements and permeate composition analyses were performed using a custom-built high pressure, high temperature permeameter [37] equipped with a calibrated SRI-3610 gas chromatograph with a thermal conductivity detector. GC calibration curves for hydrogen and carbon dioxide were generated as described in a previous work [38]. Flat membranes were loaded in a permeation cell and sealed with graphite gaskets compressed between the flat surfaces of the flanges exposing a membrane area up to 5.0 cm² [37]. The retentate was connected to a pressure regulator and mass flow controllers to adjust the stage cut (θ in Equation (1) and Fig. S1 in supplementary information) of the membrane to minimize carbon dioxide concentration polarization at the surface [38]. Typical stage cut values, expressed as % recovery, range from 0.01 (1% H2 recovery) to 1 (100% H_2 recovery), covering most of the retentate purge rates, Q_R , for a given flow rate across the membrane, Q_P , and feed rate Q_F . For calculating the stage cut, the purge, flow, and feed rates were converted to $cm_{(STP)}^3 min^{-1}$

With these considerations, the flow rate Q_P (expressed as $\mathrm{cm}_{(\mathrm{STP})}^2 \, \mathrm{s}^{-1}$) at a given differential transmembrane pressure, Δp (cmHg), was measured experimentally, and the permeability P in Barrer (1 Barrer = $1 \times 10^{-10} \, \mathrm{cm}_{(\mathrm{STP})}^3 \, \mathrm{cm} \, (\mathrm{cm}^2 \, \mathrm{s} \, \mathrm{cmHg})^{-1}$) was calculated using Equation (2), where A is the exposed area of the membrane (cm²) with thickness L (cm).

$$\theta = \frac{Q_P}{Q_P + Q_R} \tag{1}$$

$$Q_P = \frac{AP\Delta p}{I} \tag{2}$$

The determination of P was performed using the last 60% of the pressure-time curve data in the steady state region. Ideal selectivities ($a_{i/j}$) were calculated from the ratio of the permeabilities (P) of the gases $P_{i/j}$. For gas mixtures, the permeability of each component was calculated using the partial pressure of each gas in the feed mixture, the flow rate for each gas (calculated from the selectivity of the membrane to gas mixture from GC analysis and the flow rate of the permeate at the steady state), the volume of the downstream cell, the temperature, and the membrane thickness and diameter [38]. For all pure gas permeability

measurements, a minimum of 2 membranes from separate cast films were tested. The permeability of each gas was measured at least 4 times, and the average permeability calculated using the last 3 measurements. In a typical experiment, a 5.0 cm² exposed membrane area was pressurized with a feed gas at 5 bar, 15 bar, 30 bar, or 45 bar and the other side was connected to an evacuated line. The entire system was evacuated for at least 6 h at the experimental temperatures of 35 °C, 100 °C, 200 °C, or 300 °C before a 1 h leak rate test was performed. Permeability experiments with single gases at 35 °C lasted from 2 to 5 h for fast diffusing gases and up to 1 d for slow diffusing gases. Degassing times between hydrogen runs lasted for 5 h while carbon dioxide degassing times increased to 10 h. This testing protocol was repeated for each pressure increment. Permeability experiments with a H₂:CO₂ = 1:1 mixture with stage cuts of 1 and 0.1 at 30 bar and at 35 °C were performed for up to 30 d reaching a downstream pressure of 1.3 bar. During the first 7 d, the downstream was evacuated to ensure the permeate composition corresponded to the steady state. At higher temperatures, the duration of the experiments with mixed gases was reduced to 7 d (100 °C), 2 d (200 °C), and 8 h (300 °C).

The activation energy of permeation was calculated using the Arrhenius equation (Equation (3)) by fitting the data directly to an exponential regression or to a linear regression if the data was previously linearized according to Equation (4):

$$P = P_0 e^{-\frac{E_p}{RT}} \tag{3}$$

$$\ln(P) = \ln(P_0) - \frac{Ep}{RT} \tag{4}$$

where P is the permeability of the gases (Barrer), P_0 is the preexponential factor (Barrer), E_p is the activation energy of permeation (kJ mol⁻¹), R the universal gas constant (8.314 J mol⁻¹ K⁻¹), and T is the testing temperature expressed in absolute temperature units (K). It should be noted that if Equation (3) or (4) cannot describe the permeability-temperature relationship properly due to deviations from linearity, then a modified Arrhenius equation should be used [39].

Considering the temperature dependence of the diffusivity (Equation (5)) and solubility (Equation (6)), and that the permeability in polymers is the product of diffusivity times solubility (Equation (7)), the activation energy of permeation can be written as the sum of the activation energy of diffusion and the heat of sorption (Equation (8)):

$$D = D_0 e^{-\frac{Ed}{Rl}} \tag{5}$$

$$S = S_0 e^{-\frac{\Delta Hs}{RT}} \tag{6}$$

$$P = D \times S \tag{7}$$

$$E_p = E_d + \Delta H_s \tag{8}$$

where D is diffusivity, S is solubility, D_0 and S_0 are pre-exponential factors, E_d is the activation energy of diffusion (always positive), and ΔH_s is the heat of adsorption (positive or negative). Depending on the magnitude of ΔH_s , E_p could be positive or negative [40].

2.3. Fabrication of PBI membranes

The 26 wt% PBI in DMAc solution containing 1.5 wt% LiCl was diluted to 12 wt% with DMAc and stirred for a least 1 d to have homogeneous solutions for membrane fabrication. Flat, dense, free standing, PBI membranes were cast at room temperature onto provisional Mylar® substrates from 12 wt% PBI solutions in DMAc using a calibrated blade attached to an automatic applicator (Sheen 1133 N). The membranes on the Mylar® substrates were then transferred to a preheated table purged with nitrogen to dry for 2 h–3 h at 50 °C. The membranes were then removed from the Mylar® substrate, placed between glass plates with 2 mm gap, and dried in a custom-made

programmable vacuum oven. The temperature was increased to 80 °C for 12 h, then to 150 °C for 1 d, 200 °C for 12 h, and to a final temperature of either 250 °C, 300 °C, 350 °C, or 400 °C for 1 d. The thicknesses of the flat, free standing, PBI membranes ranged from 15 μm to 30 μm .

3. Results and discussion

3.1. A note on PBI synthesis

From the most common PBI synthesis procedures described in Scheme S1 in the PBI synthesis section in the supplementary information, it can be seen that incomplete elimination of the hydroxyl moiety at the C2 position (see Fig. 1 for atom numbering) from the formation of the five-member imidazole ring leads to the formation of a prepolymer, (c) in Scheme S2. The prepolymer obtained from this first step contains a combination of PBI (C2 imidazole carbon with sp² hybridization) and hydroxylated PBI segments (PBI-OH, C2 imidazole carbon with sp³ hybridization) in a PBI/PBI-OH ratio that ranges from 0.25 to 1. A second polymerization step, carried out at 360 °C-400 °C, releases water from the formation of the C=N bond in the imidazole ring in PBI-OH segments in the prepolymer and brings the C2 imidazole carbon to a trigonal planar configuration from the tetragonal configuration (Scheme S2). This second step converts the prepolymer into PBI where the C2 imidazole carbon is in a sp² hybridization state, (d) in Scheme S2. The number of PBI-OH segments remaining in PBI depends on the synthesis procedure and the temperature and duration of the thermal treatment of the polymer. If the polymer backbone contains a mixture of PBI and PBI-OH segments, then it can be predicted that during the high temperature annealing of the membranes, changes in the polymer configuration (permanent stereostructure of a polymer modified only by chemical reactions) could result in segmental motions that could change the polymer packing in the membrane in those segments.

3.2. Thermogravimetric and mass spectrum analyses

Thermogravimetric analyses of PBI membranes annealed at 250 °C, 300 °C, 350 °C, and 400 °C (Fig. 2a–d) and of the as-received PBI polymer powder (Fig. 2e) show an initial weight loss of 4%–8% at temperatures up to 180 °C that is attributed to desorbed water [41–45]. This was verified by mass spectra of the membrane annealed at 250 °C (Fig. 3), which in the 0 min–16 min time frame of the temperature program (equivalent to 150 °C–180 °C), shows water at m/z 18 as the only species released. The larger water desorption from the membrane annealed at 350 °C over the ones annealed at 250 °C or 300 °C can be attributed to the increased water sorption capacity of the membrane that results from DMAc desorption during annealing at 350 °C. As is observed in Fig. 4a, remaining DMAc (m/z 87) in the membrane starts to desorb at temperatures above 300 °C, which enables more sorption sites for water in this membrane than in membranes annealed at lower temperatures.

The total ion current (TIC) and the TIC at m/z 18 obtained from the mass spectra scans in Fig. 4a show the ion current evolution of all species and of water, respectively, in time and correlated to the temperature program. The TIC at m/z 18 shows a maximum at 150 °C and a gradual increase at temperatures up to 450 °C indicating a temperature dependence in water evolution. The mass spectrum at min 1 (Fig. 4b,i), when the temperature was 150 °C, shows molecular fragments at m/z 16, 17, 18, and 19 that correspond to water fragmentation only from electron impact ionization and not from other species. Water desorption from PBI in this temperature range was previously reported and was attributed to strong interactions of water with the imidazole rings [46–49].

The presence of lithium chloride (mp = $610\,^{\circ}$ C [50]) in the polymer solution is also a second source of adsorbed water that is released in this temperature range. According to Kamali et al. [51] and Masset et al. [50], 94% of water is desorbed from lithium chloride hydrates at 99 °C–110 °C and the remaining at 160 °C–186 °C. At temperatures

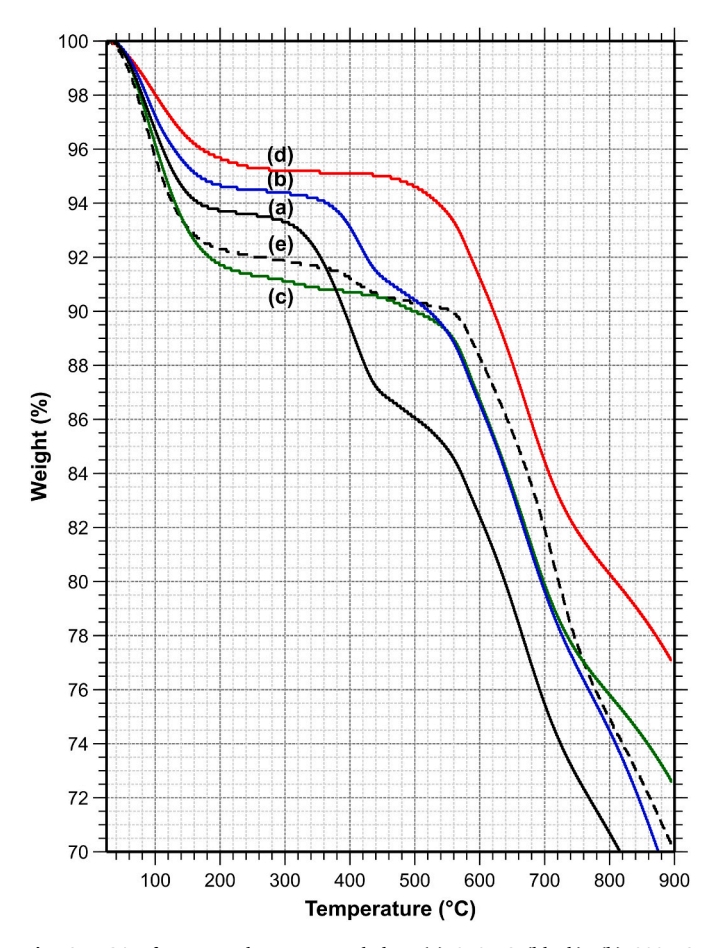


Fig. 2. TGA of PBI membranes annealed at (a) 250 $^{\circ}$ C (black), (b) 300 $^{\circ}$ C (blue), (c) 350 $^{\circ}$ C (green), (d) 400 $^{\circ}$ C (red), and (e) as received PBI powder (black dotted line). (For interpretation of the references to colour in this figure legend, the reader is referred to the Web version of this article.)

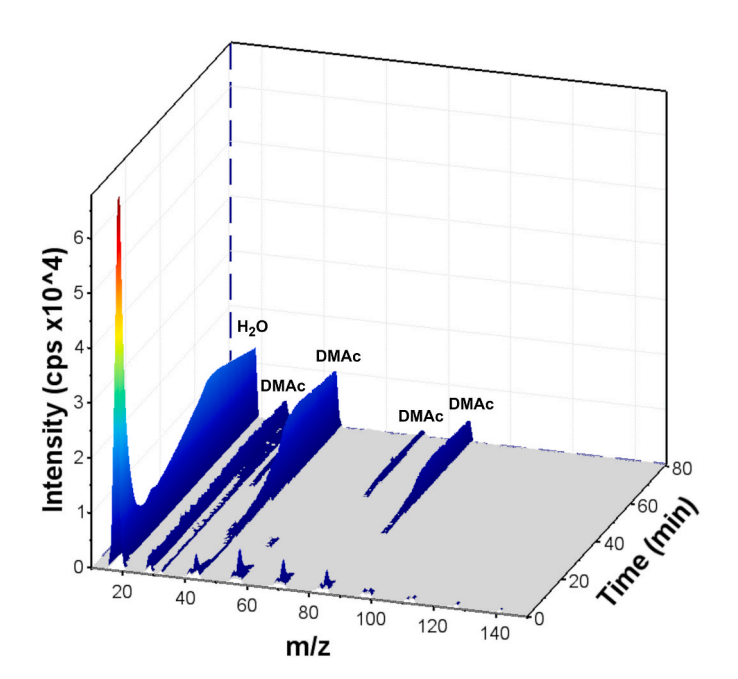
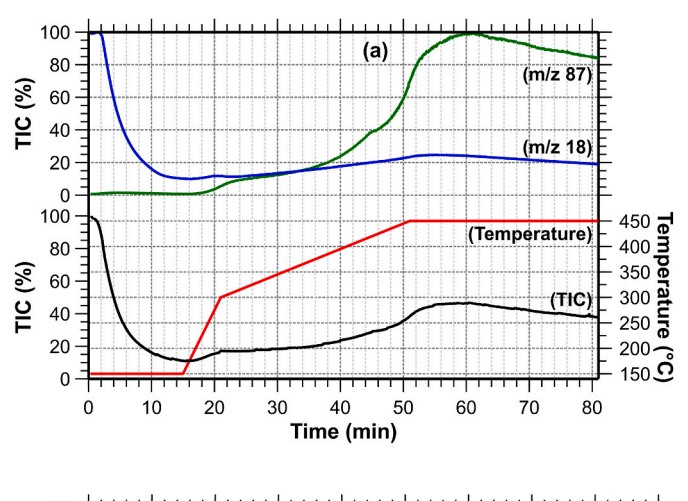


Fig. 3. High-temperature (150 °C–450 °C) mass spectra of a PBI membrane annealed at 250 °C. Temperature program: hold at 150 °C for 15 min, 150 °C–300 °C at 25 °C/min, 300 °C–450 °C at 5 °C/min, hold at 450 °C for 30 min.



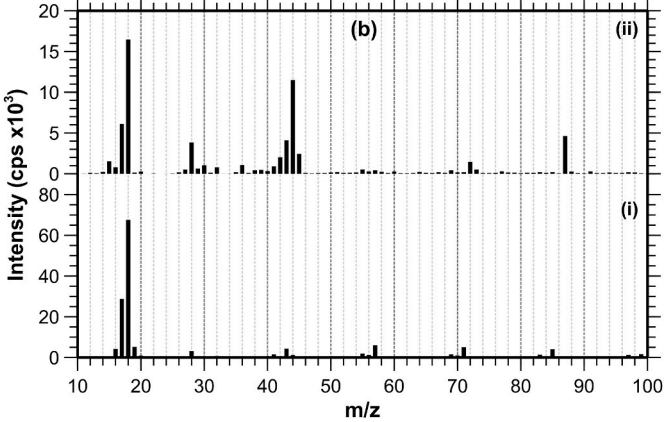


Fig. 4. a) Temperature profile, high-temperature (150 °C–450 °C) normalized TIC of all species, and normalized TICs for m/z 18 and m/z 87 obtained from mass spectra of a PBI membrane annealed at 250 °C. b) Mass spectrum at 1 min (i) and at 60 min (ii).

higher than 200 °C, no desorbed water from lithium chloride hydrates was observed [50,51]. Thermogravimetric analyses of lithium chloride at temperatures up to 1300 °C show that lithium chloride evaporates at atmospheric pressure at temperatures higher than 800 °C [51] with no water desorption from lithium chloride hydrates. For the present work, it can be concluded that all water from lithium chloride hydrates is desorbed at temperatures below 200 °C.

At temperatures higher than 180 °C, thermogravimetric analyses reveal significant differences between the PBI membrane's thermograms during a second weight loss in the 180 °C-450 °C temperature range, which depends on the membrane's annealing temperature. For membranes annealed at 250 °C, a second weight loss of 6.75% starts at 300 °C and ends at 450 °C (Fig. 2a). This weight loss is attributed to the combined loss of remaining solvent in the membrane (DMAc, bp = $165 \,^{\circ}$ C) and water released from the dehydration of hydroxylated segments that may have remained from the prepolymer formation (Scheme S2 in supporting information). This is supported by the mass spectrum obtained for this membrane, which shows that the TIC for both water (m/z)18) and DMAc (m/z 87) increase as the temperature increases from $300\,^{\circ}\text{C}$ to $450\,^{\circ}\text{C}$ (Figs. 3, 4a, 20 min–80 min segment). A mass spectrum scan at 60 min (Fig. 4b,ii), that corresponds to a temperature of 450 °C in the temperature program, shows the fragmentation pattern of water (m/z 16, 17, 18, 19) and of DMAc (m/z 15, 28, 30, 42, 43, 44, 45, 56, 72, 87, 88). A similar DMAc desorption temperature range from 200 °C to 450 °C was also observed for compatibilized PBI/polyimide blend membranes annealed at 100 °C [52]. For membranes annealed at 300 °C, the second weight loss starts at 360 °C with a 2.75% weight loss up to 450 °C (Fig. 2b), which is also attributed to the loss of remaining

DMAc from the casting solution and to water from the dehydration of PBI-OH segments (Scheme S2) that remained after the annealing at 300 °C. Since this step is slow and requires temperatures higher than 260 °C [53], annealing at 300 °C may not have fully converted the remaining PBI-OH segments from the polymer synthesis into PBI, leading to a second mass loss in the thermograms. At this annealing temperature, however, most of the PBI-OH segments may have been converted into PBI, inducing a configuration change in the polymer at the C2 imidazole carbon (Fig. 1), which changed its hybridization state from $\rm sp^3$ to $\rm sp^2$.

In the case of membranes annealed at 350 °C, a 0.5% weight loss is detected in the range of 360 °C–450 °C (Fig. 2c) that is also attributed to some water from the condensation reaction of a few PBI-OH segments that remained from the annealing and to small amounts of DMAc trapped in the membrane.

For membranes annealed at 400 $^{\circ}$ C, the polymer configuration of the PBI-OH segments may have completely converted to PBI segments due to changes in hybridization states from sp³ to sp² of the C2 carbon in the imidazole rings. In addition, DMAc was also completely removed from the membrane. For this reason, a second weight loss is not observed in this temperature range (Fig. 2d).

For the as-received polymer, a second weight loss of 1.5% was observed between 300 °C and 450 °C (Fig. 2e) that is attributed to water from the dehydration of remaining PBI-OH segments in the chains, as in the case of membranes annealed at 250 °C and 300 °C (Scheme S2). Considering a MW of 308 g/mol of the repeat unit of PBI (Fig. 1), an estimate of the number of PBI-OH segments present in the PBI polymer can be made based on the amount of water released by the PBI powder since this compound was not dissolved in DMAc. The 1.5% weight loss (or 1.5 g if the total is taken as 100 g) would translate to 83.3 mmol of water and the remaining 98.5% (98.5 g) to 319.5 mmol of PBI repeat units. In terms of moles, this means that 26% of the PBI repeat units contain one hydroxylated benzimidazole unit (a PBI-OH segment) and one benzimidazole unit, or, in terms of benzimidazole units, 13% of all the benzimidazole units present in the polymer are hydroxylated benzimidazoles. Using the estimated amount of water released from the PBI-OH segments in the powder polymer, and assuming that the annealing temperature of 250 °C did not affect the PBI-OH segments, it would be possible to estimate the amount of water and DMAc present in the membrane annealed at 250 °C. It follows that from the 6.75% (or 6.75 g) weight loss in this membrane (Figs. 2a), 5.25% or 60 mmol corresponds to DMAc (MW = 87 g/mol) and 1.5% or 83.3 mmol to water. At higher annealing temperatures, this assumption is not valid since water and DMAc could be released at different rates.

At temperatures above 450 $^{\circ}$ C, all the membranes and the asreceived polymer powder start to decompose at about 550 $^{\circ}$ C (Fig. 2) leaving a carbon film residue. It should be noted that at annealing temperatures higher than 350 $^{\circ}$ C the membranes became insoluble in DMAc, as it was also observed in a previous work [54], suggesting the possibility of a crosslinking reaction via free radical reactions [55,56] at temperatures higher than 350 $^{\circ}$ C and up to 400 $^{\circ}$ C.

The purge gas in TGA measurements also impacts the PBI thermograms. As it was shown by Belohlav [41], PBI under helium reaches thermal stabilities close to 650 $^{\circ}$ C before a significant weight loss or released species are observed in a mass spectrum. Under air, however, the thermal stability of PBI drops to 500 $^{\circ}$ C. The thermal degradation of PBI at temperatures above 450 $^{\circ}$ C was studied in more detail in previous works [41,57,58] and provide a more detailed description of the species released from the thermal decomposition of PBI.

3.3. Imaging

Fig. S2 (supplementary information) shows the optical images (Fig. S2a,d,g,j) and the SEM images (Fig. S2b,c,e,f,h,i,k,l) of the PBI membranes cross-sections at high and low magnifications. Optical images show no change in color for the membranes annealed at 250 °C,

300 °C, and 350 °C. At 400 °C, however, the membrane changed color from light brown to dark brown, indicating that changes occurred in the polymer as the annealed temperature approached the polymer's decomposition temperature ($T_d = 500$ °C, Fig. 2). This is supported by the change in solubility of the polymer at this temperature that makes the membranes completely insoluble, even after being immersed in DMAc for 2 years. SEM images (Fig. S2b,e,h,k) show the membranes have no gross defects from the casting procedure or from annealing at high temperatures. Higher magnification SEM images (Fig. S2c,f,i) show the presence of 100 nm-200 nm nodules for membranes annealed up to 350 $^{\circ}$ C. The formation of nodules has been observed in several polymers but their formation process is still debated [59]. For the membrane annealed at 400 °C, the SEM image (Fig. S21) shows induced plastic deformation from the freeze fracture and the presence of smaller nodules. These changes suggest that, at temperatures above 350 °C and up to 400 $^{\circ}$ C, PBI may undergo chemical and physical changes.

3.4. Spectroscopic characterization

3.4.1. X-ray diffraction

X-ray diffraction studies of the membranes (Fig. 5) show small shifts in the broad peak position for the membranes annealed at 250 °C and 300 °C (Fig. 5a and b). For these membranes, a shift to a lower $2\theta^\circ$ angle from 22° to 21° was observed suggesting changes in the conformation and packing of the polymer segments resulted from annealing at these temperatures. The membranes annealed at 350 °C (Fig. 5c) exhibited a shift to a higher $2\theta^\circ$ angle from 21° to 23° suggesting segmental motion

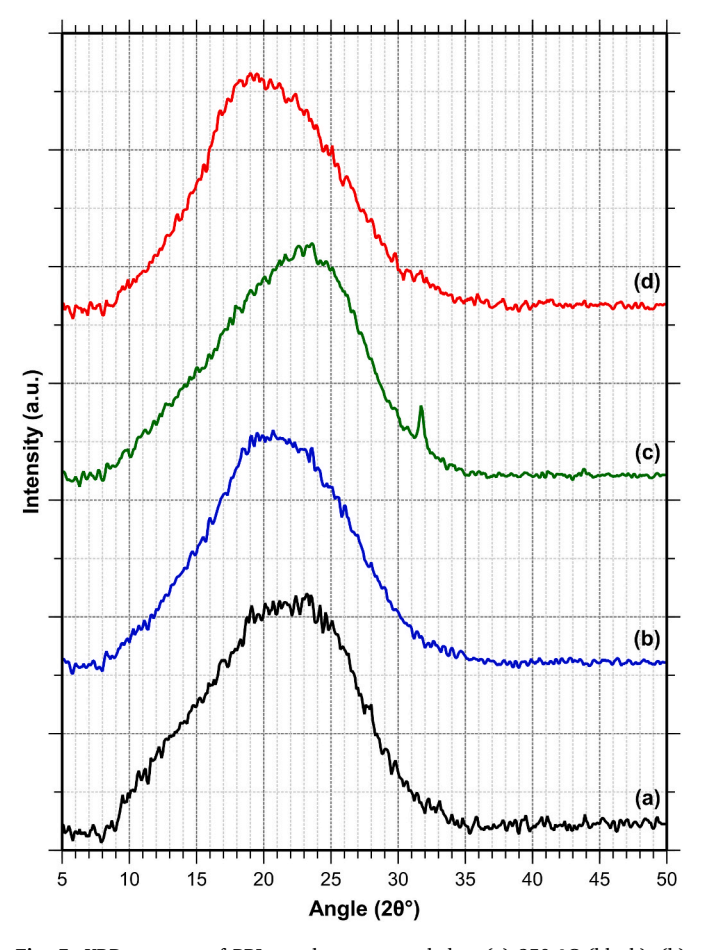


Fig. 5. XRD patterns of PBI membranes annealed at (a) 250 $^{\circ}$ C (black), (b) 300 $^{\circ}$ C (blue), (c) 350 $^{\circ}$ C (green), and (d) 400 $^{\circ}$ C (red). (For interpretation of the references to colour in this figure legend, the reader is referred to the Web version of this article.)

within the chains may have changed the chain packing. This could be the result of the elimination of water from the conversion of PBI-OH segments into PBI segments and the removal of DMAc (Figs. 2 and 4). Membranes annealed at 400 °C (Fig. 5d) show a more significant change in the diffracting angle, the 20° angle shifts from 23° to 19° , indicating a loosening of the packing that could arise from crosslinking reactions within the membrane.

3.4.2. FT-IR

Assignments of infrared absorption bands of PBI in the 400 cm⁻¹ to 4000 cm^{-1} region are reported in the open literature [21,46–49,60–67]. These assignments were performed using absorption bands for imidazole [61,68], benzimidazole, benzimidazole-metal complexes, and halogenated benzimidazoles that helped trace changes in band intensity and vibration frequency [60]. The origin of peak broadening, N-H··N hydrogen bonding, and N-H vibrations in imidazoles in the 2500 cm⁻¹ to 3600 cm⁻¹ region, upon which many bands for PBI were assigned, was reported by Zimmermann [68] from IR, Raman, and NMR studies of imidazoles, imidazole complexes, and deuterated imidazoles. The reported band assignments in the 2500 cm⁻¹ to 4000 cm⁻¹ region was performed by taking infrared spectra with increasing temperature to identify bands corresponding to aromatic C-H vibrations (3065 cm⁻¹) [48,60,64], to N-H··N polymer-polymer hydrogen bonding vibrations $(3145 \text{ cm}^{-1}) [46,48,63,64]$, to 'free' N-H vibration $(3400 \text{ cm}^{-1}) [46,48]$ 63-65], and to adsorbed water in the polymer (3623 cm⁻¹) [46-49,66,

Keeping the polymer's temperature above 120 °C while acquiring the infrared spectrum allowed researchers to observe the effect of temperature on the polymer [46,48]. Brooks et al. [46] concluded that the broad band at 3623 cm⁻¹ corresponded to the O-H stretching of adsorbed water which could be removed upon heating. This band and part of the broadening in this region disappeared when the sample was heated to 120 °C and then rescanned. Similar effects and conclusions were obtained for a series of functionalized PBIs studied by Kumbharkar et al. [47]. It was later proposed that the broadening of the band at 3623 cm⁻¹ could arise from N··H–O–H hydrogen bonding between the polymer's imidazole rings and water $(3598 \text{ cm}^{-1} - 3628 \text{ cm}^{-1})$ [46,47,49,63]. It was also observed that the intensity of the broad band at 3145 cm⁻¹ decreased with increasing temperature indicating a reduction of the N-H·N polymer-polymer interaction (interchain hydrogen bonding) [46,48,63,64]). The effect of temperature on other absorption bands was not significant but helped to assign bands for the 'free' (non-hydrogen bonded) N-H stretch at 3400 cm⁻¹ [46,48,63-65] and for the C-H aromatic stretching at 3065 cm⁻¹ [48,60,64]. The strong and broad absorption band from N··H-O-H and N-H··N hydrogen bonding could also be masking the absorption band for PBI-OH in the 3500-3600 cm⁻¹ region for membranes annealed at 250 °C [53] making it difficult to resolve it. Table S2 (supporting information) summarizes the room temperature infrared absorption bands from PBI membranes annealed at 250 °C from this work (Fig. 6a) and their assignment using reported absorption bands. Fig. 6b-d also shows the infrared spectra of the membranes annealed at 300 °C, 350 °C, and 400 °C.

High temperature thermal treatment (250 °C–350 °C) did not result in oxidation of PBI since the absorption bands at 3415 cm $^{-1}$, 3145 cm $^{-1}$, 1438 cm $^{-1}$, 1280 cm $^{-1}$, and 801 cm $^{-1}$ were not affected in intensity or shape. If oxidation would have occurred, then a considerable reduction in intensity of these absorption bands would have been detected in the spectra in this region [48]. Oxidation would also have broadened and introduced new bands (e.g., carbonyls at 1700 cm $^{-1}$) in the region 1200 cm $^{-1}$ to 1700 cm $^{-1}$ due to chemical reactions with air [48]. This effect was not observed in the spectra of the membranes from this work.

The PBI membranes annealed at 400 $^{\circ}$ C, however, showed a significant reduction in band intensity at 3145 cm $^{-1}$ which could result from a permanent disruption of N–H··N polymer-polymer hydrogen bonding. Similar changes in band absorption at 3145 cm $^{-1}$ have been observed in FT-IR spectra obtained at 350 $^{\circ}$ C, but this was attributed to a decrease in

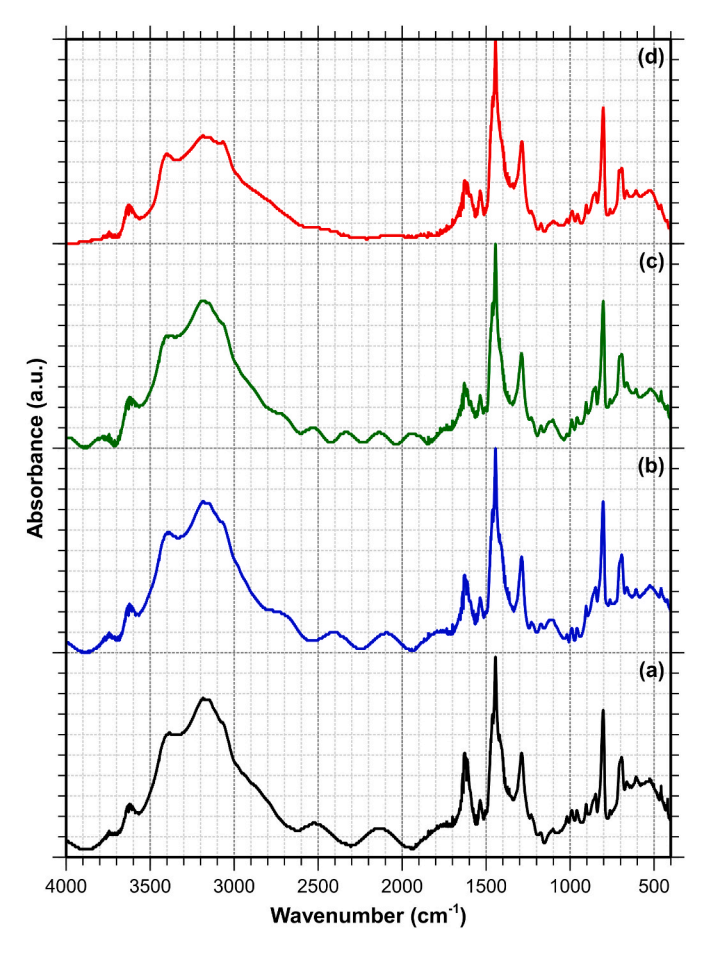


Fig. 6. FTIR spectra of PBI membranes annealed at (a) 250 $^{\circ}$ C (black), (b) 300 $^{\circ}$ C (blue), (c) 350 $^{\circ}$ C (green), and (d) 400 $^{\circ}$ C (red). (For interpretation of the references to colour in this figure legend, the reader is referred to the Web version of this article.)

the molar absorption coefficient at high temperatures and not to a decrease in N-H··N polymer-polymer hydrogen bonding [48]. This is in agreement with the room temperature FT-IR spectrum of PBI membranes annealed at 350 $^{\circ}$ C from this work that shows no change in band intensity at 3145 cm⁻¹, suggesting that the decrease in intensity observed by Musto et al. [48] was reversible and probably due to the reduction of the molar absorption coefficient. For the membranes from this work annealed at 400 °C, a reduction in molar absorptivity would not explain the decreased intensity of the 3145 cm⁻¹ band since the spectrum was obtained at room temperature. The reduced intensity of this band likely results from permanent changes in the polymer's configuration which could be associated to the crosslinking of some segments in the chains that make the membranes annealed at this temperature insoluble in DMAc and DMSO. An effect of the reduced N-H-·N polymer-polymer hydrogen bonding could be reflected in the XRD pattern for these membranes that show a shifting to a lower angle. This shifting could result from the reduction in the number of segments with N-H··N polymer-polymer hydrogen bonding in the chains and a disruption of this interaction that leads to the loosening of the packing of some segments in the chains.

For all the membranes from this work annealed between 250 $^{\circ}$ C and 400 $^{\circ}$ C, the infrared spectra at room temperature show similar relative intensities for water adsorption at 3623 cm $^{-1}$. This indicates nitrogen atoms in the imidazole rings are accessible to water at room temperature which could affect the gas permeation properties of membranes at room temperature by reducing sorption sites for CO₂ and the effective size of diffusion paths. This scenario could change in gas permeation

experiments at temperatures above 100 $^{\circ}$ C, where water would be desorbed from the membrane making sorption sites available to CO₂ and enabling diffusion paths to gas molecules that otherwise would not be accessible.

3.5. Gas permeation

3.5.1. Single gas

3.5.1.1. Effect of pressure and testing temperature on gas permeation. Single gas permeability and selectivity data for all the membranes tested in this work is summarized in Table 1 and Table S6, Fig. S3, and Fig. S4 in the supplementary information. The combination of high pressure and high temperature conditions (e.g., P=45 bar and $T=300\,^{\circ}\text{C}$) did not affect the mechanical stability of the membranes over periods of gas permeation testing of up to 30 days. Moreover, cycles of pressurization of up to 45 bar and degassing at 300 $^{\circ}\text{C}$ did not compromise the mechanical stability of the membranes, demonstrating the resilience of PBI membranes for gas separations at high pressure and high temperature. Testing the membranes at different pressures within a set temperature

also ensured the permeability properties were free of errors from defects in the membrane that could have arisen from mechanical stress induced by the high pressure and high temperature conditions.

Permeability data from Table 1 and Table S6, displayed in Fig. S3, show that permeability increased with increasing testing temperature, but mixed results were obtained when the feed pressure was increased within a set temperature. Depending upon the gas tested, permeability either remained constant or declined with increasing pressure within a set temperature. For the majority of the membranes tested at pressures above 5 bar, the permeability of hydrogen and nitrogen remained relatively constant whereas the permeability of carbon dioxide decreased with increasing pressure. For example, for a membrane annealed at 250 °C, the permeability of hydrogen at 35 °C remained at 1.5 ± 0.2 Barrer regardless of the feed pressure (5–45 bar) whereas the permeability of carbon dioxide decreased from $5 \times 10^{-2} \pm 1 \times 10^{-2}$ Barrer at 5 bar to $3 \times 10^{-2} \pm 1 \times 10^{-2}$ Barrer as the feed pressure increased to 45 bar. This effect for carbon dioxide was observed regardless of the annealing and testing temperatures (Table 1 and Table S6). This was attributed to the compaction of the membrane [69] that constrained mostly the diffusion paths for larger molecules, leaving

Table 1
Single gas (hydrogen, carbon dioxide, and nitrogen) permeabilities (Barrer)^a and ideal selectivities at different temperatures and pressures in PBI membranes annealed at 250 °C, 300 °C, or 400 °C. Permeability data obtained from first permeability cycle (5 bar–45 bar, 35 °C–300 °C).

| | Testing | Tempera | ture (°C) | | | | | | | | | | | | | |
|--|-------------|-----------------|-----------------|------------------|-----------------|-----------------|--------------|--------------|-----------|-----------|-----------|-----------|-------------|-------------|-------------|-------------|
| | 35 | | | 100 | | | | 200 | | | 300 | | | | | |
| | Feed P | ressure (b | ar) | | - | | | | | | | | | | | |
| Annealing | 5 | 15 meability | 30 | 45 | 5 | 15 | 30 | 45 | 5 | 15 | 30 | 45 | 5 | 15 | 30 | 45 |
| Temp. (°C) 250 | 1.5 | 1.5 | (Barrer) 1.5 | $1.5 \pm$ | 5.4 ± | 5.4 ± | $5.2 \pm$ | 5.4 ± | 19 ± | 20 ± | 20 ± | $20 \pm$ | 45 ± | 45 ± | 45 ± | 45 ± |
| 230 | ± 0.2 | ± 0.3 | ± 0.2 | 0.2 | 0.4 0.4 | 0.5 | 0.4 | 0.5 | 3 | 20 ± | 20 ± | 20 ± | 6 6 | 5 ± | 7 7 | 43 ± 8 |
| 300 | ± 0.2 | ± 0.3 1.0 | ± 0.2 | 0.2 0.8 ± | 4.8 ± | 0.3 4.9 ± | 0.4 4.9 ± | 5.0 ± | 3 17 ± | 2 18 ± | 2 17 ± | 2 18 ± | 45 ± | 3 45 ± | 7 46 ± | 6 45 ± |
| | ± 0.1 | ± 0.2 | ± 0.2 | 0.8 ± 0.2 | 4.6 ± 0.2 | 4.9 ± 0.1 | 4.9 ± 0.1 | 0.1 | 1/ ± 1 | 10 ± | 17 ± 1 | 10 ± | 45 ± 1 | 45 ± 1 | 40 ± 2 | 43 ± 2 |
| 400 | 1.3 | ± 0.2 | ± 0.2 1.4 | $1.5 \pm$ | 6.4 ± | 6.4 ± | 6.5 ± | 6.4 ± | 20 ± | 20 ± | 20 ± | 20 ± | 44 ± | 45 ± | 45 ± | 46 ± |
| | ± 0.5 | ± 0.5 | ± 0.4 | 1.5 ± 0.4 | 0.4 ± 0.4 | 0.4 ± | 0.3 ± 0.4 | 0.4 ± 0.3 | 20 ± 2 | 20 ± 2 | 20 ± 2 | 20 ± 2 | 7 T | 43 ± 8 | 43 ± 10 | 40 ± |
| CO ₂ Permeabi | | | ± 0.4 | 0.4 | 0.4 | 0.4 | 0.4 | 0.3 | 2 | 2 | 2 | 2 | / | 0 | 10 | 9 |
| 250 | 5 ± 1 | 4 ± 1 | 4 ± 1 | 3 ± 1 | $22 \pm$ | 22 \pm | 21 \pm | $20 \pm$ | $73 \pm$ | 76 ± | 75 ± | 76 \pm | 111 | 126 | 131 | 153 |
| 300 | 3 ± 1 | 4 I I | 4 ± 1 | 3 ± 1 | 3 | 22 ± 4 | 5 ± | 20 ± | 73 ± 5 | 70 ± 4 | 75 ± 1 | 70 ± 3 | ± 48 | \pm 52 | ± 46 | ± 9 |
| | 2.0 | 2.0 | 1.8 | $1.7 \pm$ | 3 14 \pm | 4 14 \pm | $12 \pm$ | $12 \pm$ | 50 ± | 50 ± | 49 ± | 3 49 ± | ± 46 159 | ± 32 153 | ± 40 151 | 151 |
| | ± 0.1 | ± 0.5 | ± 0.4 | 1.7 ± 0.4 | 14 ± 2 | 14 ± 2 | 12 ± 1 | 12 ± 1 | 30 ± | 30 ± | 49 ± 1 | 49 ± 1 | ± 1 | ± 1 | ± 1 | |
| | | | | $0.4 \\ 2 \pm 1$ | 23 ± | 2 21 \pm | 1 19 ± | 1 17 ± | 3 76 ± | 3 70 ± | 1 66 ± | 1 65 ± | ± 1 150 | ± 1 150 | ± 1 148 | ± 1 145 |
| 400 | 4 ± 3 | 3 ± 2 | 3 ± 1 | $Z \pm 1$ | | 21 ± 7 | | | | | | | | | | |
| N D 1:1: | . (10=3 p | | | | 9 | / | 6 | 5 | 2 | 3 | 3 | 3 | ± 20 | ± 20 | $\pm~20$ | ± 20 |
| N ₂ Permeabili | ty (x10 ° B | arrer) | | 10. | 4.4. | 15 . | 10 | 16.1 | 115 | 110 | 100 | 100 | 0.00 | 0.45 | 070 | 006 |
| 250 | | | | 1.2 ± | 14 ± | $15 \pm$ | 18 ± | 16 ± | 115 | 118 | 122 | 129 | 260 | 247 | 270 | 296 |
| | | | | 0.3 | 4 | 5 | 8 | 5 | ± 7 | ± 1 | ± 2 | ± 12 | ± 241 | ± 235 | ± 230 | ± 206 |
| 300 | | | | 0.8 ± | $9.2 \pm$ | 8.4 ± | 8.4 ± | 8.4 ± | 79 ± | 90 ± | 89 ± | 84 ± | 435 | 433 | 434 | 432 |
| | | | | 0.3 | 2.8 | 0.3 | 0.6 | 0.4 | 7 | 12 | 9 | 3 | ± 4 | ± 4 | ± 1 | ± 1 |
| 400 | | | | $1.1 \pm$ | $18 \pm$ | $16 \pm$ | $16 \pm$ | $16 \pm$ | 125 | 116 | 114 | 112 | 416 | 424 | 425 | 426 |
| | | | | 0.1 | 1 | 3 | 4 | 4 | ± 2 | ± 11 | ± 12 | ± 12 | \pm 64 | \pm 50 | \pm 52 | \pm 55 |
| H ₂ /CO ₂ Select | | | | | | | | | | | | | | | | |
| 250 | $31 \pm$ | $34 \pm$ | 42 \pm | 50 ± 6 | $25 \pm$ | $25 \pm$ | $26 \pm$ | $28~\pm$ | $26 \pm$ | $26 \pm$ | $27 \pm$ | $27 \pm$ | 44 ± | 38 \pm | $36 \pm$ | $29 \pm$ |
| | 2 | 2 | 6 | | 5 | 7 | 8 | 9 | 2 | 1 | 2 | 3 | 13 | 11 | 8 | 4 |
| 300 | 47 \pm | $51 \pm$ | 54 \pm | 49 ± 3 | $35 \pm$ | $36 \pm$ | 40 \pm | 43 \pm | $35 \pm$ | $35 \pm$ | $35 \pm$ | $36 \pm$ | $28~\pm$ | $30 \pm$ | $30 \pm$ | $30 \pm$ |
| | 2 | 5 | 1 | | 2 | 4 | 2 | 2 | 2 | 3 | 3 | 1 | 1 | 1 | 1 | 1 |
| 400 | 45 \pm | 46 \pm | 54 \pm | $66 \pm$ | $31 \pm$ | 32 \pm | $36 \pm$ | $38 \pm$ | 26 \pm | $28~\pm$ | $30 \pm$ | $31 \pm$ | $30 \pm$ | $30 \pm$ | $31 \pm$ | $32 \pm$ |
| | 23 | 11 | 10 | 23 | 11 | 9 | 9 | 9 | 2 | 4 | 5 | 5 | 1 | 2 | 2 | 2 |
| H ₂ /N ₂ Selective | vity | | | | | | | | | | | | | | | |
| 250 | | | | 1243 | 421 | 371 | 318 | 345 | 166 | 165 | 164 | 158 | 286 | 403 | 248 | 187 |
| | | | | \pm 81 | ± 149 | ± 144 | ± 151 | ± 130 | ± 13 | ± 16 | ± 18 | \pm 28 | ± 242 | \pm 400 | $\pm~188$ | $\pm~103$ |
| 300 | | | | 1132 | 547 | 578 | 588 | 592 | 217 | 195 | 197 | 211 | 103 | 104 | 105 | 104 |
| | | | | $\pm~260$ | $\pm~187$ | ± 21 | ± 39 | ± 39 | ± 19 | \pm 18 | \pm 8 | \pm 4 | ± 1 | \pm 2 | \pm 4 | \pm 4 |
| 400 | | | | 1346 | 353 | 399 | 423 | 425 | 158 | 173 | 178 | 183 | 107 | 106 | 106 | 108 |
| | | | | \pm 522 | $\pm~10$ | \pm 47 | \pm 87 | \pm 92 | $\pm~12$ | \pm 34 | \pm 37 | \pm 41 | ± 1 | \pm 8 | $\pm~10$ | \pm 7 |
| CO2/N2 Select | ivity | | | | | | | | | | | | | | | |
| 250 | | | | 25 ± 2 | $17 \pm$ | 15 \pm | 12 \pm | $12\ \pm$ | 6.4 \pm | 6.4 \pm | $6.2 \pm$ | $5.9 \pm$ | 6 ± 4 | 9 ± 8 | 7 ± 4 | 7 ± 4 |
| | | | | | 2 | 2 | 2 | 1 | 0.1 | 0.2 | 0.2 | 0.3 | | | | |
| 300 | | | | 23 ± 4 | 16 \pm | $16 \pm$ | 15 \pm | 14 \pm | 6.3 \pm | 5.6 \pm | 5.6 \pm | 5.8 \pm | 3.7 \pm | 3.5 \pm | 3.5 \pm | 3.5 \pm |
| | | | | | 6 | 1 | 1 | 1 | 0.2 | 0.9 | 0.6 | 0.1 | 0.1 | 0.1 | 0.1 | 0.1 |
| 400 | | | | $23 \pm$ | $12 \pm$ | $13 \pm$ | $12 \pm$ | $11 \pm$ | $6.0 \pm$ | $6.1 \pm$ | 5.9 ± | $5.8 \pm$ | $3.6 \pm$ | $3.5 \pm$ | $3.5 \pm$ | 3.4 \pm |
| | | | | 15 | 5 | 2 | 1 | 1 | 0.1 | 0.3 | 0.3 | 0.4 | 0.1 | 0.1 | 0.1 | 0.1 |

Average of *P* and $\alpha_{i/j}$ of 2 membranes (*P* and $\alpha_{i/j}$ for each membrane shown in Tables S3,S4,S5).

a) 1 Barrer = 1×10^{-10} cm_(STP) cm (cm² s cmHg)⁻¹.

hydrogen's diffusion paths relatively unaffected. This explains partially the trend of increasing H_2/CO_2 selectivity with increasing pressure for all the membranes tested at temperatures up to 300 °C. Although membrane compaction at high pressures offers a reasonable explanation for the increased selectivity of the membranes, it does not account for the higher H_2/CO_2 selectivity of 31 \pm 2, or 47 \pm 2, or 45 \pm 23 at 5 bar and 35 °C observed for the membranes annealed at 250 °C, 300 °C, and 400 °C, respectively. Comparing these selectivities to the ones corresponding to the majority of the membranes listed in Table S1, it can be concluded that the increased selectivity must be explained by a phenomenon other than membrane compaction, which is discussed in the following sections.

3.5.1.2. Effect of annealing temperature on gas permeation. It can be concluded from Table 1 and Table S6 that the permeabilities for hydrogen, carbon dioxide, and nitrogen of the membranes annealed at 250 °C and 400 °C are quite similar for almost any given combination of pressure and temperature, but significantly different for the membranes annealed at 300 °C. For example, for a membrane annealed at 250 °C the permeability of hydrogen at 35 $^{\circ}$ C remained at 1.5 \pm (0.2–0.3) Barrer, at 100 °C at (5.2–5.4) \pm (0.4–0.5) Barrer, at 200 °C at (19–20) \pm (2–3) Barrer, and at 300 $^{\circ}\text{C}$ at 45 \pm (5–8) Barrer. Similarly, for a membrane annealed at 400 °C the permeability of hydrogen at 35 °C remained at $(1.3 – 1.5) \pm (0.4 – 0.5)$ Barrer, at 100 °C at $(6.4 – 6.5) \pm (0.3 – 0.4)$ Barrer, at 200 °C at 20 \pm 2 Barrer, and at 300 °C at (44–46) \pm (7-10) Barrer. For membranes annealed at 300 °C, however, differences in permeability can be observed when comparing to the membranes annealed at 250 $^{\circ}\text{C}$ and 400 $^{\circ}$ C. For these membranes, the permeability of hydrogen at 35 $^{\circ}$ C remained at (0.8–1.0) \pm (0.1–0.2) Barrer, at 100 °C at (4.8–5.0) \pm (0.1–0.2) Barrer, at 200 °C at (17–18) \pm 1 Barrer, and at 300 °C at $(45-46) \pm (1-2)$ Barrer. The differences in permeability for carbon dioxide and nitrogen between membranes annealed at 300 $^{\circ}\text{C}$ and those annealed at 250 °C or 400 °C are even more significant than for hydrogen. For example, at 200 °C the permeability of carbon dioxide for membranes annealed at 250 °C is (73–76) x $10^{-2} \pm (1-5)$ x 10^{-2} Barrer, for membranes annealed at 400 °C is (65–76) x $10^{-2} \pm (2-3)$ x 10^{-2} Barrer, whereas for membranes annealed at 300 °C is (49–50) x 10^{-2} \pm $(1-3) \times 10^{-2}$ Barrer. Differences of similar magnitude are also observed for nitrogen's permeability at 200 °C: for membranes annealed at 250 °C the permeability of nitrogen is (115–129) x $10^{-3} \pm$ (1-12) x 10^{-3} Barrer, for membranes annealed at 400 $^{\circ}\text{C}$ is (112–125) x $10^{-3} \pm$ (2-12) x 10^{-3} Barrer, whereas for membranes annealed at 300 °C is (79–90) x 10^{-3} \pm $(3-12) \times 10^{-3}$ Barrer. These differences in permeability point to the possibility that different annealing temperatures may affect the membranes' permeability properties in different ways. Taking the annealing temperature of 250 °C as reference, it can be observed that membranes annealed at 300 °C may have less free volume as a result of a better packing due to the removal of adsorbed water, to microscopic segmental motions from the higher conversion of PBI-OH segments to PBI segments induced by the high temperature, and to the removal of some remaining DMAc. As the annealing temperature increases to 400 °C a total conversion from PBI-OH segments to PBI is achieved. In addition, a complete DMAc removal and an increase in free volume due to bond breaking/formation during crosslinking could have been achieved which results in an increase in permeability. Microscopic changes in segmental orientation in polymer conformation at high annealing temperatures is possible since the removal of solvent, adsorbed water, and water from the dehydration of PBI-OH may allow for segments to move freely into a conformation with lower energy. The ideal scenario of such polymer conformation would be the crystallization of segments in the polymer where the planar PBI chains would stack into a tightly packed ordered structure. Such an ideal scenario was modeled for PBI by Y. Wang et al. [70] and found that in PBI, carbon dioxide and nitrogen would experience two different diffusion paths with significant energy barriers. Diffusion across the chains would have higher energy barrier

 $(\mathrm{CO_2}=1.40~\mathrm{eV},\,\mathrm{N_2}=1.05~\mathrm{eV})$ than diffusion parallel to the chains $(\mathrm{CO_2}=0.52~\mathrm{eV},\,\mathrm{N_2}=0.71~\mathrm{eV}).$ It is then plausible to infer that the presence of adsorbed molecules (e.g., DMAc), and potentially the presence of hydrogen bonding between chains and to water, occurring at these positions, would significantly impact parallel diffusion of gas molecules between polymer layers. Added to these changes in packing, is the effect of the increased number of available sorption sites after the high temperature annealing, which quickly adsorb water from the environment during membrane handling and storage. Adsorbed water, as is described below, plays an important role in gas permeation in PBI at temperatures below $100~^{\circ}\mathrm{C}$.

3.5.1.3. Effect of adsorbed water on gas permeation. To understand the effect of water on gas permeation in PBI, the permeability and selectivity to carbon dioxide was analyzed. The larger variability in carbon dioxide permeation at 35 °C between different pressures, and among the membranes annealed at different temperatures, could be the source of the observed variability in H2/CO2 selectivities observed in Table 1, Table S1, and Table S6. Since carbon dioxide has two orders of magnitude lower permeability than hydrogen, it can be safely inferred that its permeability will be more sensitive to small changes in polymer packing and diffusional paths than hydrogen's permeability. This in turn will be readily reflected in the H2/CO2 selectivity of the membrane. The variability in permeability, especially at temperatures below 100 $^{\circ}\text{C},$ can be attributed to the amount of adsorbed water and remaining DMAc, which depend on the annealing temperature and storage conditions. This is plausible since for all the membranes tested in this work, the permeability of the gases converged to similar values at temperatures above 100 °C. The only change in the membranes in testing up to 100 °C. regardless of the annealing temperature, is the desorption of water from the membranes which ranged from 4% to 8% (Fig. 2). A seemingly small amount of 5% adsorbed water would translate into 1 molecule of water adsorbed per PBI repeating unit (MW = 308 g/mol), and at 8% the amount of water could increase up to 2 molecules per repeating unit. This amount of water is significant since a maximum of 2-4 water molecules could be adsorbed per repeating unit, depending on whether the water molecules act as a proton donor and acceptor or as a simultaneous donor/acceptor. In the first case, one water molecule would act as a proton donor and a second water molecule as a proton acceptor when hydrogen bonding to each nitrogen in the repeat unit, giving a maximum of 4 adsorbed water molecules per repeating unit. If the water molecule is hydrogen bonding to two nitrogen atoms from two chains, then it would be acting as a proton donor and acceptor, limiting the amount of water adsorbed to 2 molecules per repeating unit [46]. Which case is taking place in the membranes is difficult to assess. Since the amount of adsorbed water depends, among other factors, on the history of the membrane (e.g., storage conditions, membrane handling, relative humidity) it is then possible to conclude that water would be adsorbed by the membranes in different amounts. The amount of water adsorbed by the membranes from this work fall within the theoretical limits described above and has an impact on the permeation properties of the membranes. The impact of water could be even more dramatic for low permeable gases (e.g., carbon dioxide, nitrogen) since these gases are more sensitive to changes in sorption sites and diffusion paths than the more permeable gases (e.g., hydrogen). Adsorbed water can also impact disproportionally the permeabilities of fast and slow diffusion gases in PBI by inducing plasticization of the membrane, as it was recently reported [34].

At testing temperatures lower than 200 $^{\circ}$ C, water may still be adsorbed in sorption sites that otherwise would be available for carbon dioxide adsorption, impacting its transport across the membrane and therefore the selectivity of the membrane for gas pairs involving carbon dioxide. The amount of water adsorbed would depend on the number of sorption sites available in the membrane, which could be affected by the thermal treatment. For membranes annealed at 300 $^{\circ}$ C and 400 $^{\circ}$ C, the

thermal treatment removed partially or all the remaining DMAc molecules, potentially left fewer to none PBI-OH segments, and made available sorption sites in the imidazole rings. These sorption sites, however, are quickly occupied by water adsorbed from the environment during the removal of the membranes from the oven, storage, and mounting. If crosslinking proceeded at 400 $^{\circ}\mathrm{C}$ then it can be also concluded that water and carbon dioxide sorption sites in the membrane were significantly reduced, impacting the gas transport of carbon dioxide at testing temperatures below 200 $^{\circ}\mathrm{C}$.

As water was desorbed from the membranes during the permeation experiments when the temperature was increased above 100 °C, the permeability of the gases for the membranes annealed at 250 °C, 300 °C, and 400 °C converged into similar values, especially when the testing temperature approached 300 $^{\circ}$ C, where all the membranes had similar permeability properties. To understand the effect of water and the conditioning of the membrane on gas permeation, membranes annealed at 400 $^{\circ}\text{C}$ were subjected to permeability experiments from 35 $^{\circ}\text{C}$ to 300 °C and then brought back to 35 °C for a second permeability cycle up to 300 °C. The results (Table S6) show that the performance of the membranes was more reproduceable at lower temperatures during the second cycle than in the first cycle, presumably due to complete removal of adsorbed water. Permeabilities also increased by 35% for hydrogen and 100% for carbon dioxide and nitrogen. At testing temperatures above 100 °C, the membranes performed similarly in the first and second permeation cycles. These results show the effect of water on the permeability properties of PBI at temperatures below 100 °C and also show the difficulty in removing it from the membranes, requiring temperatures up to 150 °C to remove it completely from the membrane [42, 43,71,72]. The results suggest that the membranes may require a conditioning period that includes removal of adsorbed water and remaining DMAc if the annealing temperature is less than 350 °C before achieving a stable state and exhibiting true permeability properties.

3.5.1.4. Combined effects on gas selectivity. A clear picture emerges when ideal selectivity (Table 1, Table S6, and Fig. S4) is incorporated in the gas permeation analysis. For membranes annealed at 250 °C, and depending on the pressure, the H₂/CO₂ selectivity at 35 °C ranges from 31 ± 2 to 50 ± 6 but quickly drops to 25 ± 5 to 28 ± 9 at $100\,^{\circ}\text{C}$ and remains relatively constant up to 300 °C. A similar trend is observed for membranes annealed at 300 $^{\circ}\text{C}$ and 400 $^{\circ}\text{C}$ where the H₂/CO₂ selectivities start at higher values at 35 °C (H $_2$ /CO $_2$ 47 \pm 2 to 66 \pm 23) and then, between 100 $^{\circ}\text{C}$ and 300 $^{\circ}\text{C},$ drop between 28 \pm 1 and 43 \pm 2. The CO₂/N₂ selectivity, however, experienced a continued decrease with increasing temperature from (23–25) \pm (2-15) at 35 °C to (3.4–9) \pm (0.1–8) at 300 $^{\circ}$ C. The reason the CO₂/N₂ selectivity drops significantly lies on the rapid increase of nitrogen permeability with increasing temperature, whereas carbon dioxide's permeability increased 75-fold from 35 to 300 °C, nitrogen's permeability increased 400-fold, about 5 times the rate of increase in permeability of carbon dioxide at 300 °C. A similar trend was observed for the H₂/N₂ selectivity for which the selectivity decreased from (1132-1346) \pm (260-522) at 35 $^{\circ}\text{C}$ to (103–403) \pm (1–400) at 300 °C. It should be noted that the larger deviations mostly originated from the membranes annealed at 250 °C rather than from the membranes annealed at 300 °C or 400 °C.

The effect of water and DMAc desorption from the membranes on selectivity after the first temperature cycle was also observed on membranes annealed at 400 °C (Table 1 and Fig. S4c,f,i). The $\rm H_2/CO_2$ selectivity of these membranes remained relatively constant from 26 ± 5 to 31 ± 1 at 35 °C and 300 °C, respectively, revealing the direct effect water has on permeation and selectivity. The removal of water and DMAc from the membrane resulted in an increased permeability for the gases at the expense of a reduced selectivity.

Considering the effects of pressure, adsorbed water and DMAc, and annealing and testing temperatures, it can be concluded that each of these factors affect the gas transport in PBI membranes. Moreover, the magnitude of some of these factors may become dynamic as the testing temperature increases to values higher than the annealing temperature. If the testing temperature is higher than the annealing temperature then water and DMAc could be desorbed from the membranes during long degassing periods leading to a reduction in hydrogen bonding between the polymer chains and the enabling of new diffusion paths.

Membrane compaction and adsorbed water and DMAc reduces permeability whereas high testing temperatures increase permeability by increasing the thermal motion of segments in the polymer, by desorbing water and DMAc, and by eliminating hydrogen bonding between polymer chains. The effect of the membrane's annealing temperature cannot be neglected also since the data show large differences in permeability between membranes annealed at 300 $^{\circ}\text{C}$ and those annealed at 250 $^{\circ}\text{C}$ or 400 $^{\circ}\text{C}$. The conformational and configurational changes introduced by the annealing temperature may be as important as the other factors as well.

3.5.1.5. Performance of PBI membranes. To illustrate the impact of the annealing temperature and of the testing temperature on permeability and selectivity, the data obtained in this work (Table 1 and Table S6) was compared to those of the PBI membranes listed in Table S1. The resulting plots for single gas permeability (Fig. 7a-c) and ideal selectivity (Fig. 7d-f) show that the permselectivity properties of the PBI membranes of this work are more reproducible than of those from Table S1. In all permeability and selectivity plots in Fig. 7a-f, it can be seen that the largest variations in permselectivity properties come from testing temperatures lower than 100 °C. The largest differences observed are for carbon dioxide and nitrogen permeabilities with permeabilities up to 100 times greater than the ones obtained in this work. Such differences in permeability affect in similar ways the corresponding H₂/ CO₂, H₂/N₂, and CO₂/N₂ selectivities at testing temperatures lower than 100 $^{\circ}$ C. For all the PBI membranes from this work these selectivities are significantly higher than the selectivities for PBI membranes from Table S1. The fact that the membranes from this work outperform those from Table S1 demonstrates the importance of annealing PBI membranes at temperatures higher than 300 °C.

A comparison of the performance of the PBI membranes for ideal H₂/ CO₂ separations at 45 bar from this work (Table 1 and Table S6) to those of PBI membranes from Table S1 was performed using a 2008 Robeson plot [73] (Fig. 8a). Since the membranes were tested at 35 °C, 100 °C, 200 °C, and 300 °C, upper bounds for each of these temperatures were required in order to perform a fair comparison. Experimental upper bounds for this separation at temperatures higher than 35 °C are non-existent in the open literature, but updated versions of theoretical upper bounds [74,75] for up to 200 °C [28] were used to draw the upper bounds for H₂/CO₂ separations. Fig. 8a shows that all the PBI membranes from this work tested at 35 °C, 100 °C, 200 °C, or 300 °C performed above either the 2008 Robeson upper bound (35 $^{\circ}\text{C--50}$ $^{\circ}\text{C}$) or above the theoretical upper bounds (100 $^{\circ}$ C, 200 $^{\circ}$ C, 300 $^{\circ}$ C). The plots show that the majority of the membranes from Table S1 lie below the upper bound for membranes tested at 35 °C, whereas the membranes of this work lie above this bound. This is remarkable since at this temperature the membranes were affected by adsorbed water and DMAc and yet performed significantly better than the membranes from Table S1. The most significant difference is the higher annealing temperatures of the membranes from this work, which according to Fig. 8a, improved significantly the performance of the membranes. The performance of the membranes tested at 100 °C, 200 °C, and 300 °C were also significantly better than those from Table S1 although a smaller set of membranes tested at these temperatures was available for comparison. Fig. 8a also shows that at testing temperatures of up to 200 °C, the selectivity properties of membranes annealed at 300 or 400 °C were higher than those of membranes annealed at 250 $^{\circ}$ C. This could be due to the effect that residual DMAc and water has in the membranes, as was discussed above in the single gas permeation sections, and to the

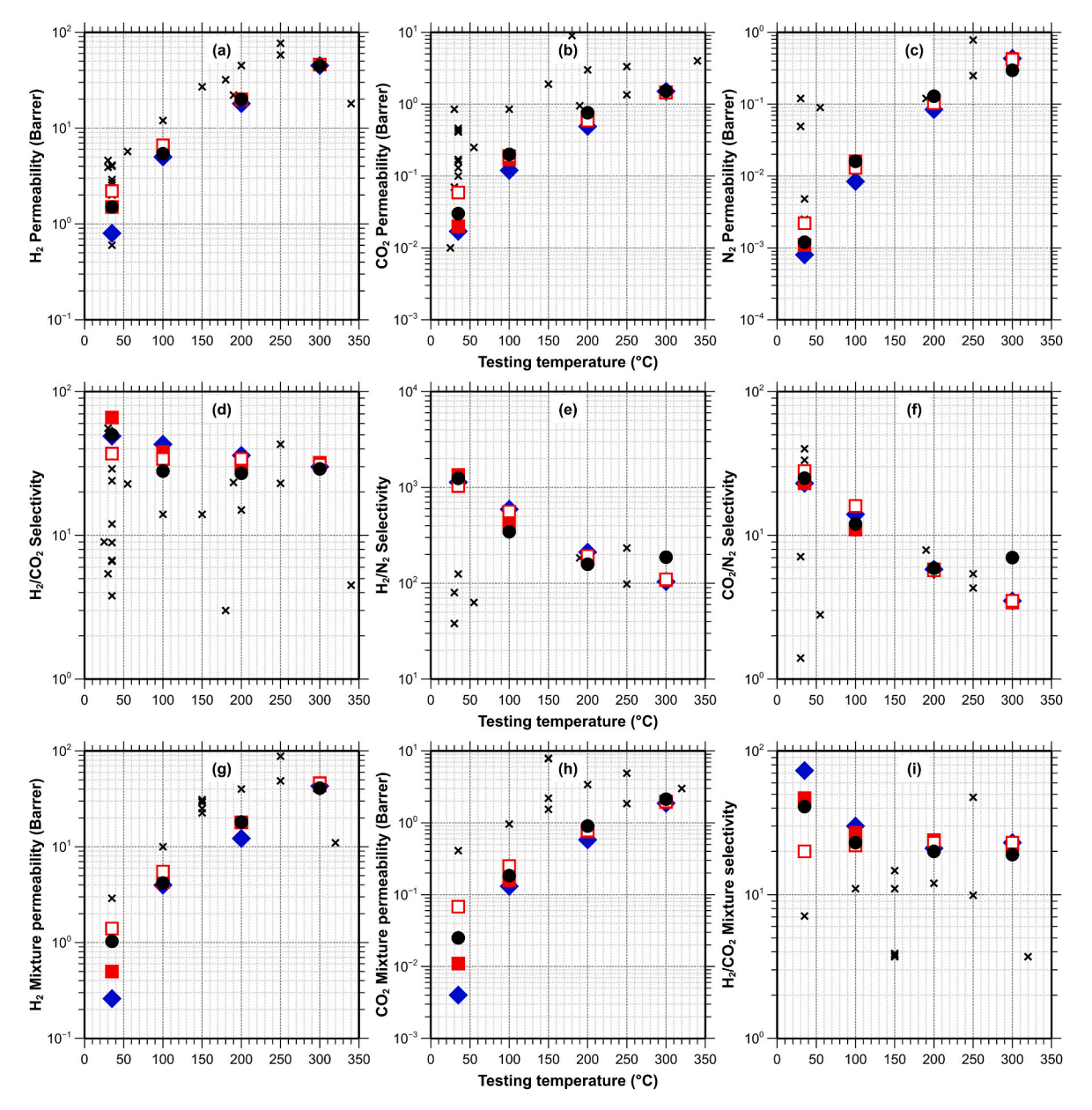


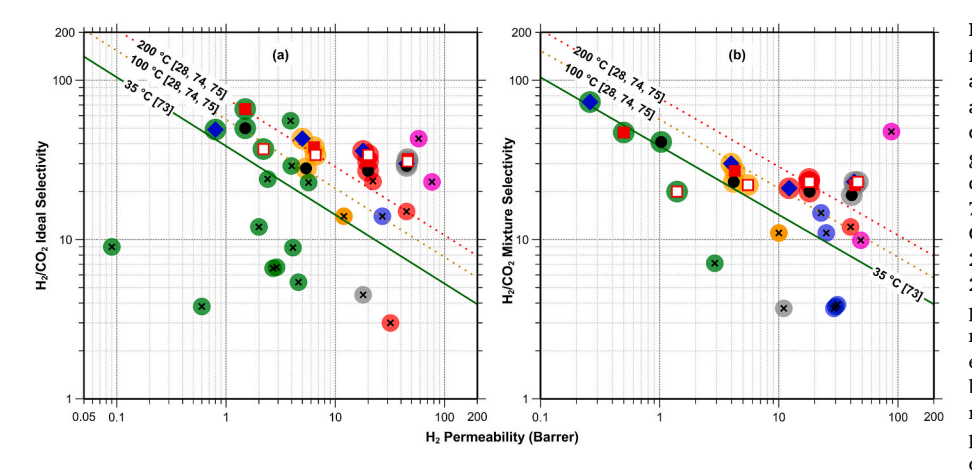
Fig. 7. Comparison of PBI membranes separation properties at 45 bar from this work (\bullet , \bullet , \blacksquare , \square) to those of membranes annealed at different temperatures (x) from Table S1. Pure gas permeabilities (a–c), ideal selectivities (d–f), and gas mixture (H₂:CO₂ = 1:1) separation at 30 bar and stage cut of 0.1 (g–i) for PBI membranes annealed at 250 °C (\bullet), 300 °C (\bullet), or 400 °C (\blacksquare , \square). Full symbols represent permeability properties from the first permeability cycle. For membranes annealed at 400 °C, open (\square) symbols represent permeability properties from the second permeability cycle for pure gases or the average of the second and third permeability cycles for gas mixtures. Data from Table 1 and Tables S1,S6,S7,S8. (For interpretation of the references to colour in this figure legend, the reader is referred to the Web version of this article.)

possibility that DMAc limited an efficient packing of the polymer at annealing temperatures up to 250 $^{\circ}\text{C},$ therefore impacting the membrane's selectivity.

3.5.1.6. Activation energy of permeation. The activation energy of permeability (E_p) and the pre-exponential factor (P_0) at 45 bar for hydrogen, carbon dioxide, and nitrogen were calculated using Equation (3) and data from Table 1 and Table S6. The data (permeability vs. 1/T) was plotted in a logarithmic scale (Fig. S5 in supplementary information) and visually inspected to verify the plots were linear. The data was then fitted to an exponential regression from which P_0 and E_p were obtained (Table 2). In analyzing E_p values, one must remember that for dense membranes, the diffusion component of the activation energy (Equation (8)) depends on the size of the penetrant [76–79] and that the

mobility of gas molecules in polymers largely depend on the available free volume in the polymer which, for the membranes in this work, may change according to the annealing temperature.

The high annealing temperatures help remove remaining solvent (DMAc) and adsorbed water, induce microscopic movements of segments, induce dehydration reactions (Scheme S2), and probably induce crosslinking, thus affecting the E_p for the gases tested in this work. Table 2 shows that the E_p for all the gases tested in all the membranes increases as the size of the gas molecules increases with $E_{pH2} < E_{pCO2} < E_{pN2}$. For example, for membranes annealed at 300 °C the E_{pH2} (22.0 kJ/mol) $< E_{pCO2}$ (24.4 kJ/mol) $< E_{pN2}$ (34.7 kJ/mol), following the trend described in Refs. [76,77] with increasing penetrant size. For membranes annealed at 250 °C a similar trend is observed but with lower E_p values, the E_{pH2} (18.9 kJ/mol) $< E_{pCO2}$ (21.7 kJ/mol) $< E_{pN2}$ (30.9



to the Web version of this article.)

Fig. 8. H₂/CO₂ upper bound plots showing the performance of PBI membranes from this work annealed at 250 °C (●), 300 °C (♦), or 400 °C (■, □) (Table 1 and Tables S6,S7,S8), and of those annealed at different temperatures (x) from Table S1: (a) pure gases, (b) $H_2:CO_2 = 1:1$ mixture. Upper bounds: dotted and dashed lines for theoretical bounds [28, 74, 751 and solid lines for 2008 Robeson bounds [73]. Color backgrounds represent testing temperatures: 20-50 °C (•), 100 °C (•), 150 °C (•), 200 °C (•), 250 °C (a), and 300-350 °C (a). Pressure: 45 bar for pure gases and 30 bar and stage cut of 0.1 for H2:CO2 mixtures. Full symbols represent permeability properties from the first permeability cycle. For membranes annealed at 400 °C, open (_) symbols represent permeability properties from the second permeability cycle for pure gases in (a) or the average of the second and third permeability cycles for gas mixtures in (b). (For interpretation of the references to colour in this figure legend, the reader is referred

Table 2 Pre-exponential factor (P_0 , in Barrer) and activation energy of permeation (E_p , in kJ/mol) for pure gases in PBI membranes annealed at 250 °C, 300 °C, or 400 °C. Values calculated at 45 bar using permeability data from Table 1 and Table S6.

| Annealing Temperature (°C) | P _{0, H2} | $E_{p, H2}$ | P _{0,} CO2 | $E_{p,}$ | P _{0, N2} | E _{p, N2} |
|----------------------------|--------------------|-------------|------------------------|----------|--------------------|--------------------|
| 250 | 2401 | 18.9 | 173 | 21.7 | 257 | 30.9 |
| 300 | 4902 | 22.0 | 259 | 24.4 | 602 | 34.7 |
| 400 | 2406 | 18.7 | 238 | 23.5 | 449 | 32.6 |
| 400 ^a | 1477 | 16.7 | 55 | 17.6 | 175 | 29.1 |

^a From second permeability cycle of a PBI membrane annealed at 400 °C (Table S6).

kJ/mol). The E_p values of the membranes annealed at 250 °C suggest the membranes had lower or no microscopic segmental motion during the annealing process to achieve a more efficient packing than the membranes annealed at 300 °C. For membranes annealed at 400 °C, the E_p changes with penetrant size holds, giving E_{pH2} (18.7 kJ/mol) $< E_{pCO2}$ (23.5 kJ/mol) $< E_{pN2}$ (32.6 kJ/mol) values for the first permeability cycle, similar to those of the membranes annealed at 250 °C. This is

attributed to the physical and chemical changes these membranes underwent during the annealing (e.g., segmental motion, crosslinking), which may have increased their free volume, and to the adsorbed water from handling the membrane that reduced the diffusion of the gases during the first permeation cycle. During the second permeation cycle, the membranes annealed ad 400 $^{\circ}\text{C}$ were free of adsorbed water and possessed more accessible paths for the gas molecules to diffuse than in the first cycle thus lowering the E_p . For the second cycle the E_p drops to E_{pH2} (16.7 kJ/mol) $< E_{pCO2}$ (17.6 kJ/mol) $< E_{pN2}$ (29.1 kJ/mol), similar to those reported by Stevens et al. [29]. The E_p values obtained in this work are within the range of E_p values (-18 kJ/mol to 75 kJ/mol) of more than 400 polymers reported in the literature [40]. In the work of Alders et al. [40], the E_p values of permanent gases in a variety of polymers remained within three distinct bounds drawn in an E_p -P plot (Fig. 9), the values obtained in this work fall within these bounds. In Fig. 9, proximity to bound 1 indicates a material has either a high diffusional barrier or a low gas solubility, therefore a high E_p and a low permeability is observed for these materials. Proximity to bound 2 corresponds to materials with lower E_p and higher permeabilities, and proximity to bound 3 indicates the possibility the material has low resistance to gas diffusion. For nitrogen, the E_{pN2} values lie closely to the

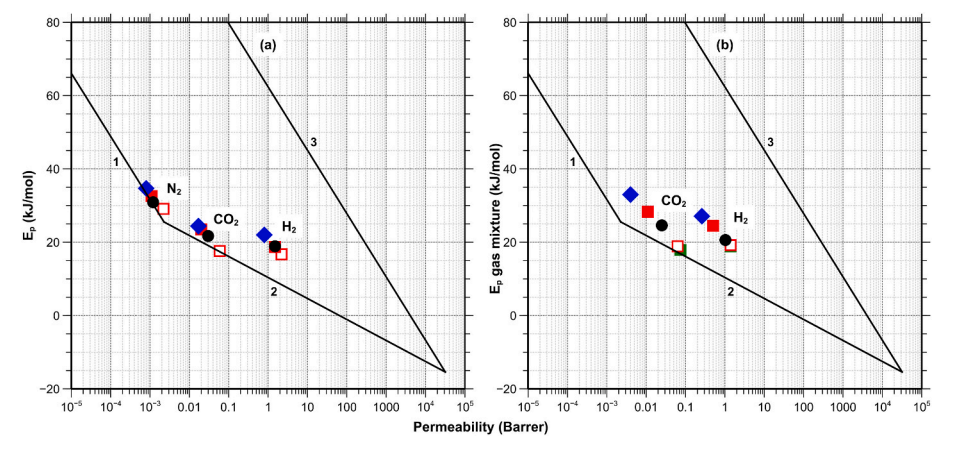


Fig. 9. Activation energy of permeation – permeability plots for hydrogen, carbon dioxide, and nitrogen from PBI membranes annealed at 250 °C (●), 300 °C (•), or 400 °C (■, □, ■): (a) pure gases at 45 bar (Table 2), (b) $H_2:CO_2 = 1:1$ mixture at 30 bar and stage cut of 0.1 (Table S9). Upper and lower bounds from [40]. Full symbols (except ■) represent E_p and P properties from the first permeability cycle. For membranes annealed at 400 °C, open (□) and (■) symbols represent properties from the second and third permeability cycles, respectively. (For interpretation of the references to colour in this figure legend, the reader is referred to the Web version of this article.)

lower end of bound 1 where barrier materials are located with high E_n and lower P values. For hydrogen and carbon dioxide, however, the E_{pH2} and E_{pCO2} values lie more closely to bound 2 (Fig. 9a) where most of polyimides and polymers of intrinsic microporosity (PIM) lie. This indicates the membranes act as barrier materials for molecules larger than carbon dioxide and as a permeable membrane for smaller gas molecules. Fig. 9a also shows that all the membranes possess low E_p and low Pvalues for all the gases tested. A low E_p and a low P combination for a gas maybe counterintuitive but as shown in the work of Alders et al. [40] this is not uncommon for several polymers. For hydrogen, for example, the low E_{pH2} and the low P_{H2} result from the presence of a small number of diffusional paths (e.g., free volume, microvoids) with void sizes small enough for hydrogen to diffuse but not large enough for carbon dioxide and nitrogen to diffuse freely thus reducing carbon dioxide and nitrogen's permeability significantly more than for hydrogen's, this may explain the high H₂/CO₂ and H₂/N₂ selectivities observed for PBI membranes from this work at both low and high temperatures. Because there is a small number of these diffusional paths, the permeability of hydrogen is low and also sensitive to the presence of water, DMAc, and fluctuations in segmental motions in the chains. Since water (kinetic diameter = 0.265 nm) can diffuse more easily than hydrogen (kinetic diameter = 0.289 nm) into the membrane's sorption sites present in the highly selective diffusional paths, the permeability of hydrogen is impacted despite its low E_{pH2} . An interesting observation that supports this conclusion is the similar magnitude of E_{pH2} and E_{pCO2} obtained from the second permeability cycle for the membrane annealed at 400 °C. At this annealing temperature, the membrane is free of adsorbed water and DMAc but still retains a large H₂/CO₂ selectivity and low gas permeabilities when compared to other membranes (e.g., polyimides, PIM-1), as is observed in Fig. 8a. The fact that a relatively low E_p for hydrogen, carbon dioxide, and nitrogen were obtained indicates that these gases do not require large amounts of energy to jump or diffuse across polymer chains, but once they do, they encounter a limited number of microvoids that allow them to diffuse. In the case of PBI, the walls of the microvoids must be stiffer and more size-selective (higher sieving capabilities) to retain selectivity at high temperatures than in other polymers (e.g., polyimides) therefore increasing the selectivity of the membrane for smaller molecules.

3.5.2. Gas mixture

The gas separation performance of the PBI membranes with gas mixtures ($H_2\text{:}CO_2=1\text{:}1)$ resembled that of the pure gases. It was noted that even though the permeabilities of the gases were low, the total flowrate across the membranes was significant to induce concentration polarization on the membranes which reduced their H_2/CO_2 selectivities when the stage cut was 1 (no retentate removal or 100% hydrogen recovery), this was even more significant at temperatures above $100\,^{\circ}\text{C}$. For example, for the PBI membrane annealed at 400 $^{\circ}\text{C}$, the average H_2/CO_2 mixture selectivities of the second and third permeation cycles with a stage cut of 1 were 18 ± 1 at $35\,^{\circ}\text{C}$, 19 ± 1 at $100\,^{\circ}\text{C}$, 13 ± 1 at $200\,^{\circ}\text{C}$, and 10 ± 1 at $300\,^{\circ}\text{C}$. In contrast, when the retentate was removed from the feed at a stage cut of 0.1 (10% hydrogen recovery) the high H_2/CO_2 selectivity of PBI was recovered.

Following the example of the PBI membrane annealed at 400 °C, the average H_2/CO_2 mixture selectivities of the second and third permeation cycles with a stage cut of 0.1 were 20 ± 1 at 35 °C, 22 ± 1 at 100 °C, 23 ± 1 at 200 °C, and 23 ± 1 at 300 °C. Similar trends were observed for the membranes annealed at 250 °C and at 300 °C. Therefore, all the analysis for gas mixture permeation relies on permeability data obtained at a stage cut of 0.1. An optimal stage cut for a maximum hydrogen recovery and high purity can be obtained by repeating this experiment at different stage cut values until a desired purity and recovery is obtained but it is beyond the scope of this work.

3.5.2.1. Effect of adsorbed water and testing temperature on gas mixture permeation. The effect of adsorbed water in PBI membranes in gas mixture permeation was similar to that observed from pure gas permeation experiments, it resulted in the lowering of the permeability of the gases and the increase of the selectivity at temperatures below 100 °C during the first permeability cycle. Hydrogen permeabilities as low as 0.26 Barrer and $\rm H_2/CO_2$ selectivities of up to 73 at 35 °C and 30 bar were observed for a PBI membrane annealed at 300 °C (Fig. 10, Table S7 and Table S8). As the testing temperature increased above 100 °C, the $\rm H_2/CO_2$ selectivity of the membranes to gas mixtures stabilized between 19 and 23 due to the desorption of water from the membrane during the first permeability cycle (Fig. 10i and Table S7).

The conditioning or stabilizing effect on permeability and selectivity due to water removal observed for pure gases was observed for gas mixtures as well. When a membrane annealed at 400 $^{\circ}$ C was tested with a H₂:CO₂ (1:1) gas mixture, the obtained permeabilities were lower and the selectivities higher at temperatures lower than 100 $^{\circ}$ C for the first permeability cycle, when comparing to the second and third permeability cycles. For the second and third permeability cycles, however, the permeability and selectivity properties stabilized and became more reproducible showing higher permeabilities and constant H₂/CO₂ selectivities (Fig. 10i and Table S8).

By comparing the pure and gas mixture separation performance of the membranes annealed at 400 °C, Table S6 and Table S8, respectively, it can be observed that the $\rm H_2/CO_2$ selectivity and hydrogen permeability from the gas mixture were lower than those from pure gases. To perform a fair comparison between pure and gas mixtures, the partial pressure of 15 bar for each gas in the $\rm H_2:CO_2$ (1:1) mixture at a total pressure of 30 bar was used. From comparing the permeability of hydrogen at 15 bar from the second permeability cycle from pure gases (Table S6) to that of the average of the second and third permeability cycles from gas mixtures (Table S8), it is observed that the permeability of hydrogen decreased significantly at temperatures lower than 200 °C.

The permeability of carbon dioxide, however, increased significantly at temperatures above 35 °C resulting in a 30% decrease in the H₂/CO₂ selectivity of the membrane from values in the order of 30-32 (pure gases at 35 °C, 100 °C, 200 °C, 300 °C and at 15 bar, Table S6) down to 20–23 (gas mixture at 35 °C, 100 °C, 200 °C, 300 °C and 30 bar with partial pressures of 15 bar for both hydrogen and carbon dioxide, Table S8). Upon removal of adsorbed water from the membrane, a significant amount of diffusion paths larger than the kinetic diameter of carbon dioxide became available to this gas thus increasing its diffusivity in the membrane. For hydrogen, however, the removal of water did not necessarily translate in a large increase of diffusional paths since most of the time microvoids were already available to it but not to carbon dioxide. The removal of water may have restored the size of the microvoids but not the quantity available in the membrane. In the absence of carbon dioxide, therefore, pure hydrogen diffuses through all the available microvoids resulting in higher permeability. In the presence of carbon dioxide, the number of available microvoids for hydrogen to diffuse gets reduced due to the diffusion of carbon dioxide through the newly enabled microvoids, free of adsorbed water, thereby lowering the permeability of hydrogen in the mixture. Another interesting observation resulting from comparing pure to gas mixture data is the steady increase in carbon dioxide's permeability from gas mixtures with increasing temperature (Table S8) when compared to pure gases (Table S6). At temperatures higher than 100 °C, only carbon dioxide's permeability from gas mixtures increased by 30% over the permeability of carbon dioxide from pure gases. Hydrogen's permeability from gas mixtures, on the other hand, approached that of from pure gases as the testing temperature increased. These observations suggest that the 30% decrease in H₂/CO₂ selectivity observed from gas mixtures may be due to the increased permeability of carbon dioxide from the mixture. How is it that the permeability of carbon dioxide from the mixture is higher than that from the pure gases? One possible explanation could lie on the effect that hydrogen diffusion has on carbon dioxides' diffusion. As

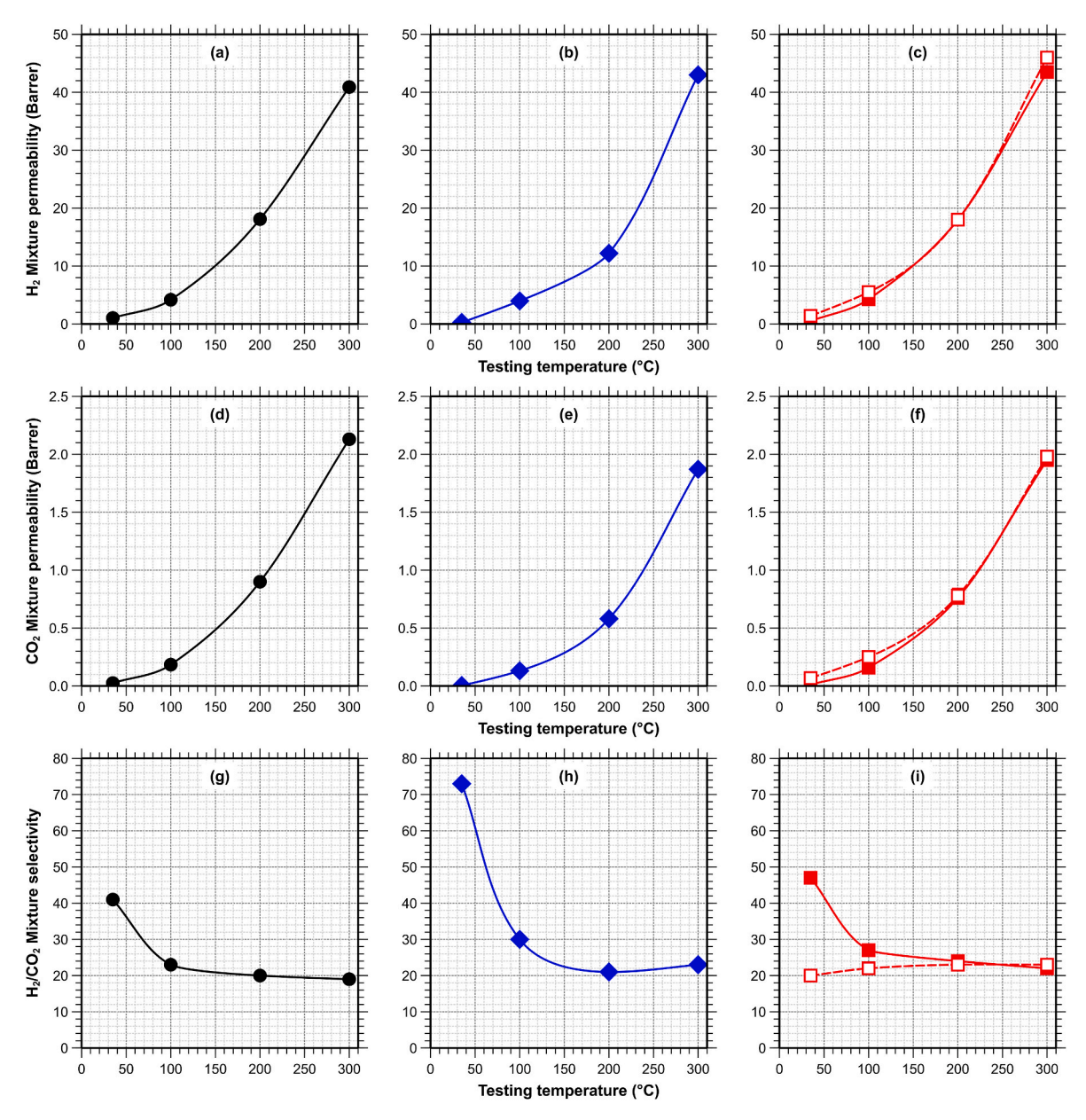


Fig. 10. Gas mixture ($H_2:CO_2 = 1:1$) separation at 30 bar and stage cut of 0.1 for PBI membranes annealed at 250 °C (\bullet in a,d,g), 300 °C (\bullet in b,e,h), or 400 °C (\blacksquare in c, f,i) using data from Table S7 and Table S8 (a-f) permeability, (g-i) H_2/CO_2 selectivity. For PBI membranes annealed at 400 °C, dashed lines with empty symbols (\square) represent permeability (c,f) and selectivity (i) averages from the second and third permeability cycles. (For interpretation of the references to colour in this figure legend, the reader is referred to the Web version of this article.)

hydrogen diffuses through some of the microvoids with sizes larger than carbon dioxide's kinetic diameter, it could be dragging carbon dioxide with it therefore enhancing carbon dioxide's permeability. This would result in a lowering of the energy barrier for diffusion for carbon dioxide in the mixture and therefore a reduction in the value of E_{pCO2} .

3.5.2.2. Effect of annealing temperature on gas permeation. Table S7 shows that the gas mixture permeabilities and selectivities for hydrogen and carbon dioxide of the membranes annealed at 250 °C and 400 °C are similar, but quite different to those of membranes annealed at 300 °C. This same behavior was observed when these membranes were tested with pure gases. Using the gas mixture permeability properties of the membrane annealed at 250 °C as reference, it can be concluded that the membrane annealed at 300 °C has less free volume than the membranes annealed at 250 °C or 400 °C since it exhibits significantly lower permeabilities and higher $\rm H_2/CO_2$ selectivities for gas mixtures (Table S7).

For this membrane, a H_2/CO_2 selectivity of 73 with a low hydrogen permeability of 0.26 Barrer was achieved for a $H_2:CO_2$ (1:1) mixture at 35 °C and 30 bar. As the testing temperature increased to 300 °C, the selectivity dropped to 23 but still remained slightly higher than the selectivities of the membranes annealed at 250 °C or 400 °C. This behavior is attributed to a better chain packing from microscopic segmental motions induced by the high annealing temperature and the removal of water and DMAc from the membrane. For the membrane annealed at 400 °C, the high annealing temperature may have crosslinked some chains and induced more microscopic segmental motions that lead to an increase in free volume during bond breaking/formation. The polymer packing changes increased the gas permeability of the membrane more than that of the membrane annealed at 300 °C.

3.5.2.3. Performance of PBI membranes with gas mixture. The gas mixture permeabilities obtained in this work (Table S7 and Table S8)

were compared to those from gas mixtures of the PBI membranes listed in Table S1. The gas mixture permeability (Fig. 7g and h) and selectivity (Fig. 7i) data show that the permselectivity properties for the PBI membranes of this work are more reproducible and are less dispersed than those from Table S1. Fig. 7g and h also shows that the permeabilities of hydrogen and carbon dioxide from this work are lower than of those from Table S1, which is attributed to the higher annealing temperatures that induced a close packing of the chains making the membranes more selective for $\rm H_2/CO_2$ than the membranes from Table S1. It is interesting to see that all the membranes form this work exhibited higher and reproducible $\rm H_2/CO_2$ selectivities (Fig. 7i) for gas mixtures than those from Table S1 at any given testing temperature, suggesting the importance of high annealing temperatures.

A comparison of the performance of the PBI membranes from this work for H₂/CO₂ mixture separations at 30 bar (Table S7 and Table S8) to those of PBI membranes from Table S1 was performed using a 2008 Robeson plot [73] (Fig. 8b). Since the membranes were tested at 35 °C, 100 °C, 200 °C, and 300 °C with a H₂:CO₂ mixture, upper bounds for each of these temperatures from H2:CO2 mixtures are required in order to perform a fair comparison. Experimental upper bounds from gas mixtures for this separation are non-existent in the open literature, instead theoretical upper bounds for pure gases up to 300 °C [28,74,75] were used to draw the upper bounds in an effort to have an approximate reference for gas mixtures at high temperatures. Fig. 8b shows that all the PBI membranes from this work tested at 35 °C, 100 °C, 200 °C, or 300 °C performed above either the 2008 Robeson upper bound at 35-50 °C or close to the theoretical upper bounds at 100 °C, 200 °C, or 300 °C. Fig. 8b also shows that almost all of the membranes from Table S1 were outperformed by the membranes from this work at any given testing temperature and membrane annealing temperature. This is remarkable since the most significant difference between the membranes from this work and those from Table S1 is the higher annealing temperatures used for the membranes prepared in this work, which according to Fig. 8b, improved significantly the performance of the membranes. Considering that gas mixture selectivity is usually lower than ideal selectivity, Fig. 8b shows a remarkable performance of the membranes from this work by performing close to the upper limits of the theoretical upper bounds for pure gases.

3.5.2.4. Activation energy of permeation from gas mixture. Calculation of the E_p and P_0 for hydrogen and carbon dioxide from a H_2 : CO_2 (1:1) mixture permeation data at 30 bar was performed in a similar fashion than for pure gases. Using Equation (3) and data from Table S7 and Table S8, the permeability for each gas from the mixture permeation in each membrane annealed at different temperature was plotted against 1/T in a logarithmic scale (Fig. S6 in supplementary information). After a visual inspection to verify the plots were linear, the data was fitted to an exponential regression from which P_0 and E_p were obtained (Table S9).

Comparison of the activation energy of permeabilities of membranes annealed at the same temperatures from Table 2 (E_p for pure gases) and from Table S9 (E_D for gas mixtures) shows that, independent of the annealing temperature, E_p from the first permeation cycles for gas mixtures is higher than the E_p for pure gases from the first permeation cycles. For the second and third permeation cycles of the membrane annealed at 400 °C, the E_D values from the mixture (Table S9) drop to values similar to those of the second permeation cycle with pure gases (Table 2). This suggests that a strong competition for diffusion paths between hydrogen and carbon dioxide may be at play when water is adsorbed in the membrane. Since water is strongly adsorbed in PBI and slowly desorbs at temperatures higher than 100 °C, it reduces the number of available diffusion paths for hydrogen and carbon dioxide and forces the gases to compete for these sites which in turn results in a lower permeability and a higher E_p for each gas. After water is desorbed during the first permeation cycle, the competition for diffusion paths in

the second and third permeability cycles decreases resulting in a lower E_n .

Comparing the effects of the annealing temperature of the membrane on E_p from gas mixtures (Table S9) to those on E_p from pure gases (Table 2), it can be seen that the E_p follows the same trend: the E_p from gas mixtures of membranes annealed at 250 °C ($E_{DH2} = 20.6$ kJ/mol, $E_{DCO2} = 24.6 \text{ kJ/mol}$) are similar to those of membranes annealed at 400 °C (E_{pH2} = 24.5 kJ/mol, E_{pCO2} = 28.3 kJ/mol) and that the E_p of both membranes are smaller than the E_p of the membranes annealed at 300 °C $(E_{pH2}=27.1 \text{ kJ/mol}, E_{pCO2}=33.0 \text{ kJ/mol})$. These variations in E_p are attributed to the same effects observed for pure gases: annealing temperatures above 350 °C removed DMAc and adsorbed water and induced microscopic movements of segments and probably crosslinking. The E_n values for the membranes annealed at 250 °C and 400 °C suggest that these membranes may have more free volume as a result of the thermal treatment than the membranes annealed at 300 °C, which may be experiencing a more compact packing than the other membranes. These physical changes would affect both pure and gas mixtures equally since the resulting conformation and configuration of the polymer in the membranes are impacted to some degree by the thermal treatment.

It can also be seen that the E_n of the gases from mixtures from the first permeation cycle increases for all membranes as the size of the gas molecules increases with $E_{pH2} < E_{pCO2}$. For the second and third cycles this does not hold, $E_{pH2} > E_{pCO2}$. For example, for membranes annealed at 400 °C the E_{pH2} (24.5 kJ/mol) $< E_{pCO2}$ (28.3 kJ/mol) for the first permeation cycle, but the E_{pH2} (18.9 kJ/mol) > E_{pCO2} (17.9 kJ/mol) for the third permeation cycle. As it can be seen, the E_{pCO2} becomes smaller than the E_{DH2} for the second and third permeability cycles, contrary to that for pure gases. In addition to the initial reduction of the E_{DCO2} due to the desorption of water, a further decrease in E_{pCO2} can be attributed to the effect of dragging that hydrogen exerts on carbon dioxide, as hydrogen diffuses and opens diffusion paths it drags carbon dioxide molecules with it, therefore lowering the E_{pCO2} . This is plausible since the permeability of carbon dioxide increased by as much as 30% with increasing temperature. Membrane plasticization is unlikely to be a factor since at high testing temperatures the solubility of carbon dioxide in the membranes is minimal and the H2/CO2 selectivity remains unchanged.

The E_p values obtained from gas mixture in this work remained within the range of E_p values (-18 kJ/mol to 75 kJ/mol) of more than 400 polymers reported in the literature [40]. As it was mentioned in the previous section, it was observed that the E_p values of permanent gases in a variety of polymers remained within three distinct bounds drawn in an E_p - P plot [40], the values obtained from gas mixtures in this work fall within these bounds. For hydrogen, the E_{pH2} values from gas mixtures remained close to bound 2 but, depending on the annealing temperature and permeation cycle, the E_{pCO2} values dispersed between bounds 1 and 2 (Fig. 9b). Taking the gas mixture permeation and E_p data from the first permeability cycle, it can be seen that the E_{pCO2} values for membranes annealed at 250 °C or 400 °C increase with increasing annealing temperature more rapidly for gas mixtures than for pure gases, but they remain close to bound 2. There is, however, the effect of better chain packing for the membrane annealed at 300 °C than for membranes annealed at 250 °C or 400 °C that moves the E_{pCO2} for this membrane from bound 2 to bound 1. These effects more likely are the result of the intense competition between hydrogen and carbon dioxide for diffusion paths due to the presence of adsorbed water that reduced the size of some diffusion paths. For the second and third permeability cycles, water is desorbed and therefore more diffusion paths are available, lowering the E_{pCO2} values within bound 2. As it can be observed from Fig. 9b, the annealing temperature plays also an important role in determining the size and availability of diffusion paths, which in conjunction with adsorbed water, impact more the E_p for gas mixtures than for pure gases.

4. Conclusions

Permeability experiments with pure hydrogen, carbon dioxide, nitrogen, and H2:CO2 mixtures revealed that two main factors affect the permeability and selectivity properties of PBI membranes: the annealing temperature and the presence of adsorbed water in the membrane. In order to obtain reproducible gas permeation data for this polymer, these two factors need to be addressed and specified when permeation data is reported. To address the issue of the annealing temperature it is recommended that the temperature must be high enough to ensure the membranes are free of impurities, residual solvent, and that the configuration of the polymer is close to 100% that of PBI (maximum conversion of prepolymer to PBI). An annealing temperature between 350 °C and 400 °C showed to be more effective in cleaning and stabilizing the membranes than lower temperatures. Addressing the issue of adsorbed water in the membranes requires a permeability cycle at temperatures higher than 100 °C, preferably close to 200 °C in order to remove the tenaciously adsorbed water from the membranes. This treatment showed to be important in obtaining higher permeabilities and reproducible selectivities, free of interferences.

The results also showed that the annealing temperature induced changes in the packing of the polymer that affected the activation energy of the gases tested. As the annealing temperature increased from 250 $^{\circ}$ C to 400 $^{\circ}$ C, the activation energies for hydrogen and carbon dioxide decreased from 18.9 (kJ/mol) to 16.7 (kJ/mol) and from 21.7 (kJ/mol) to 17.6 (kJ/mol), respectively. The changes in activation energy of permeation suggest the annealing temperature may be an important variable to consider when testing PBI membranes.

Author statement

All authors contributed equally in the manuscript preparation.

Declaration of competing interest

The authors declare that they have no known competing financial interests or personal relationships that could have appeared to influence the work reported in this paper.

Data availability

Data will be made available on request.

Acknowledgments

The authors would like to thank Miss Verena Kempkes for translating and assisting in the interpretation of Ref. [68].

This material is based upon work supported by the National Science Foundation under Grant No. CBET-1917747.

Appendix A. Supplementary data

Supplementary data to this article can be found online at https://doi.org/10.1016/j.memsci.2023.121619.

References

- [1] J. Conti, P. Holtberg, J.A. Beamon, S. Napolitano, A.M. Schaal, J.T. Turnure, L. Westfall, International Energy Outlook 2013, U.S. Energy Information Administration, DOE/EIA-0484, 2013.
- [2] D.A.J. Rand, R.M. Dell, Hydrogen Energy: Challenges and Prospects, The Royal Society of Chemistry, Cambridge, UK, 2008.
- [3] C. Acar, I. Dincer, Hydrogen energy, in: I. Dincer (Ed.), Comprehensive Energy Systems, Elsevier, Oxford, 2018, pp. 568–605.
- [4] C. Acar, I. Dincer, Hydrogen production, in: I. Dincer (Ed.), Comprehensive Energy Systems, Elsevier, Oxford, 2018, pp. 1–40.

- [5] A. Hellman, K. Honkala, S. Dahl, C.H. Christensen, J.K. Norskov, Ammonia synthesis: state of the bellwether reaction, in: J.R. Poeppelmeier (Ed.), Comprehensive Inorganic Chemistry II, Elsevier, Amsterdam, 2013, pp. 459–474.
- [6] D.C.C. Habgood, A.F.A. Hoadley, L. Zhang, Techno-economic analysis of gasification routes for ammonia production from Victorian brown coal, Chem. Eng. Res. Des. 102 (2015) 57–68.
- [7] I. Dincer, Y. Bicer, Ammonia production, in: I. Dincer (Ed.), Comprehensive Energy Systems, Elsevier, Oxford, 2018, pp. 41–94.
- [8] E. Shoko, B. McLellan, A.L. Dicks, J.C.D. da Costa, Hydrogen from coal: production and utilisation technologies, Int. J. Coal Geol. 65 (3–4) (2006) 213–222.
- [9] G.Q. Lu, J.C. Diniz da Costa, M. Duke, S. Giessler, R. Socolow, R.H. Williams, T. Kreutz, Inorganic membranes for hydrogen production and purification: a critical review and perspective, J. Colloid Interface Sci. 314 (2) (2007) 589–603.
- [10] J.J. Marano, J.P. Ciferino, Integration of gas separation membranes with IGCC identifying the right membrane for the right job, Energy Proc. 1 (1) (2009) 361–368.
- [11] K. Babita, S. Sridhar, K.V. Raghavan, Membrane reactors for fuel cell quality hydrogen through WGSR – review of their status, challenges and opportunities, Int. J. Hydrogen Energy 36 (11) (2011) 6671–6688.
- [12] F. Gallucci, E. Fernandez, P. Corengia, M. van Sint Annaland, Recent advances on membranes and membrane reactors for hydrogen production, Chem. Eng. Sci. 92 (0) (2013) 40–66.
- [13] J.C. Diniz da Costa, G.P. Reed, K. Thambimuthu, High temperature gas separation membranes in coal gasification, Energy Proc. 1 (1) (2009) 295–302.
- [14] D.S. Newsome, The water-gas shift reaction, Catal. Rev. 21 (2) (1980) 275-318.
- [15] D. Driscoll, B. Morreale, L. Headley, NETL Test Protocol: Testing of Hydrogen Separation Membranes, U.S. Department of Energy - National Energy Technology Laboratory, DOE/NETL-2008/1335, 2008.
- [16] S.C. Kumbharkar, P.B. Karadkar, U.K. Kharul, Enhancement of gas permeation properties of polybenzimidazoles by systematic structure architecture, J. Membr. Sci. 286 (1–2) (2006) 161–169.
- [17] X. Li, R.P. Singh, K.W. Dudeck, K.A. Berchtold, B.C. Benicewicz, Influence of polybenzimidazole main chain structure on H₂/CO₂ separation at elevated temperatures, J. Membr. Sci. 461 (2014) 59–68.
- [18] J.R. Klaehn, C.J. Orme, E.S. Peterson, T.A. Luther, M.G. Jones, A.K. Wertsching, J. M.U. Klaehn, CO₂ Separation Using Thermally Optimized Membranes: A Comprehensive Project Report, Idaho National Laboratory, Idaho Falls, 2000-2007. INL/EXT-07-12376, March 2008.
- [19] S.S. Araya, F. Zhou, V. Liso, S.L. Sahlin, J.R. Vang, S. Thomas, X. Gao, C. Jeppesen, S.K. Kaer, A comprehensive review of PBI-based high temperature PEM fuel cells, Int. J. Hydrogen Energy 41 (46) (2016) 21310–21344.
- [20] A. Kalathil, A. Raghavan, B. Kandasubramanian, Polymer fuel cell based on polybenzimidazole membrane; a review, Polym. Plast. Technol. Eng. (2018) 1–33.
- [21] K. Hwang, J.-H. Kim, S.-Y. Kim, H. Byun, Preparation of polybenzimidazole-based membranes and their potential applications in the fuel cell system, Energies 7 (3) (2014) 1721–1732.
- [22] D.R. Pesiri, B. Jorgensen, R.C. Dye, Thermal optimization of polybenzimidazole meniscus membranes for the separation of hydrogen, methane, and carbon dioxide, J. Membr. Sci. 218 (1–2) (2003) 11–18.
- [23] J.R. Klaehn, E.S. Peterson, A.K. Wertsching, C.J. Orme, T.A. Luther, M.G. Jones, Polybenzimidazole Compounds, US20090012253.
- [24] S.S. Hosseini, M.M. Teoh, T.S. Chung, Hydrogen separation and purification in membranes of miscible polymer blends with interpenetration networks, Polymer 49 (6) (2008) 1594–1603.
- [25] T. Yang, T.-S. Chung, High performance ZIF-8/PBI nano-composite membranes for high temperature hydrogen separation consisting of carbon monoxide and water vapor, Int. J. Hydrogen Energy 38 (1) (2013) 229–239.
- [26] A. Naderi, A. Asadi Tashvigh, T.-S. Chung, M. Weber, C. Maletzko, Molecular design of double crosslinked sulfonated polyphenylsulfone/polybenzimidazole blend membranes for an efficient hydrogen purification, J. Membr. Sci. 563 (2018) 726–733.
- [27] A. Naderi, A. Asadi Tashvigh, T.-S. Chung, H₂/CO₂ separation enhancement via chemical modification of polybenzimidazole nanostructure, J. Membr. Sci. 572 (2019) 343–349.
- [28] L. Zhu, M.T. Swihart, H. Lin, Tightening polybenzimidazole (PBI) nanostructure via chemical cross-linking for membrane H₂/CO₂ separation, J. Mater. Chem. 5 (37) (2017) 19914–19923.
- [29] K.A. Stevens, J.D. Moon, H. Borjigin, R. Liu, R.M. Joseph, J.S. Riffle, B.D. Freeman, Influence of temperature on gas transport properties of tetraaminodiphenylsulfone (TADPS) based polybenzimidazoles, J. Membr. Sci. 593 (2020), 117427.
- [30] J. Sanchez-Lainez, B. Zornoza, S. Friebe, J. Caro, S. Cao, A. Sabetghadam, B. Seoane, J. Gascon, F. Kapteijn, C. Le Guillouzer, G. Clet, M. Daturi, C. Tellez, J. Coronas, Influence of ZIF-8 particle size in the performance of polybenzimidazole mixed matrix membranes for pre-combustion CO₂ capture and its validation through interlaboratory test, J. Membr. Sci. 515 (2016) 45–53.
- [31] J. Sánchez-Laínez, B. Zornoza, M. Carta, R. Malpass-Evans, N.B. McKeown, C. Tellez, J. Coronas, Hydrogen separation at high temperature with dense and asymmetric membranes based on PIM-EA(H₂)-TB/PBI blends, Ind. Eng. Chem. Res. 57 (49) (2018) 16909–16916.
- [32] K.A. Berchtold, R.P. Singh, J.S. Young, K.W. Dudeck, Polybenzimidazole composite membranes for high temperature synthesis gas separations, J. Membr. Sci. 415–416 (2012) 265–270.
- [33] G.J. Dahe, R.P. Singh, K.W. Dudeck, D. Yang, K.A. Berchtold, Influence of nonsolvent chemistry on polybenzimidazole hollow fiber membrane preparation, J. Membr. Sci. 577 (2019) 91–103.

- [34] J.D. Moon, H. Borjigin, R. Liu, R.M. Joseph, J.S. Riffle, B.D. Freeman, D.R. Paul, Impact of humidity on gas transport in polybenzimidazole membranes, J. Membr. Sci. 639 (2021), 119758.
- [35] J. Sánchez-Laínez, B. Zornoza, C. Tellez, J. Coronas, Asymmetric polybenzimidazole membranes with thin selective skin layer containing ZIF-8 for H₂/CO₂ separation at pre-combustion capture conditions, J. Membr. Sci. 563 (2018) 427–434.
- [36] B.P. Biswal, H.D. Chaudhari, R. Banerjee, U.K. Kharul, Chemically stable covalent organic framework (COF)-polybenzimidazole hybrid membranes: enhanced gas separation through pore modulation, Chem. Eur J. 22 (14) (2016) 4695–4699.
- [37] E.V. Perez, K.J. Balkus Jr., J.P. Ferraris, I.H. Musselman, Instrument for gas permeation measurements at high pressure and high temperature, Rev. Sci. Instrum. 84 (6) (2013), 065107.
- [38] E.V. Perez, G.J.D. Kalaw, J.P. Ferraris, K.J. Balkus Jr., I.H. Musselman, Amine-functionalized (Al) MIL-53/VTEC™ mixed-matrix membranes for H₂/CO₂ mixture separations at high pressure and high temperature, J. Membr. Sci. 530 (2017) 201, 212
- [39] T. Turanyi, A.S. Tomlin, Analysis of Kinetic Reaction Mechanisms, Springer-Verlag, Berlin. 2014.
- [40] M. Alders, C. von Bargen, A. Konig, M. Wessling, Chilled membranes efficient gas permeation at sub-ambient temperatures, J. Membr. Sci. 576 (2019) 171–181.
- [41] L.R. Belohlav, Poly(benzimidazole), Angew. Makromol. Chem. 40 (1) (1974) 465–483.
- [42] J.D. Moon, M. Galizia, H. Borjigin, R. Liu, J.S. Riffle, B.D. Freeman, D.R. Paul, Water vapor sorption, diffusion, and dilation in polybenzimidazoles, Macromolecules 51 (18) (2018) 7197–7208.
- [43] T.-S. Chung, A critical review of polybenzimidazoles, J. Macromol. Sci. Rev. Macromol. Chem. Phys. 37 (2) (1997) 277–301.
- [44] M. Pishnamazi, A. Marjani, M. Pishnamazi, P.P. Selakjani, S. Shirazian, A thermokinetic model for penetrant-induced swelling in polymeric membranes: water in polybenzimidazole membranes, J. Mol. Liq. 317 (2020), 114000.
- [45] J.D. Moon, M. Galizia, H. Borjigin, R. Liu, J.S. Riffle, B.D. Freeman, D.R. Paul, Modeling water diffusion in polybenzimidazole membranes using partial immobilization and free volume theory, Polymer 189 (2020), 122170.
- [46] N.W. Brooks, R.A. Duckett, J. Rose, I.M. Ward, J. Clements, An n.m.r. study of absorbed water in polybenzimidazole, Polymer 34 (19) (1993) 4038–4042.
- [47] S.C. Kumbharkar, U.K. Kharul, New N-substituted ABPBI: synthesis and evaluation of gas permeation properties, J. Membr. Sci. 360 (1–2) (2010) 418–425.
- [48] P. Musto, F.E. Karasz, W.J. MacKnight, Fourier transform infra-red spectroscopy on the thermo-oxidative degradation of polybenzimidazole and of a polybenzimidazole/polyetherimide blend, Polymer 34 (14) (1993) 2934–2945.
- [49] S.C. Kumbharkar, U.K. Kharul, N-substitution of polybenzimidazoles: synthesis and evaluation of physical properties, Eur. Polym. J. 45 (12) (2009) 3363–3371.
- [50] P.J. Masset, Thermogravimetric study of the dehydration reaction of LiCl·H₂O, J. Therm. Anal. Calorim. 96 (2) (2009) 439–441.
- [51] A.R. Kamali, D.J. Fray, C. Schwandt, Thermokinetic characteristics of lithium chloride, J. Therm. Anal. Calorim. 104 (2) (2011) 619–626.
- [52] J.D. Moon, A.T. Bridge, C. D'Ambra, B.D. Freeman, D.R. Paul, Gas separation properties of polybenzimidazole/thermally-rearranged polymer blends, J. Membr. Sci. 582 (2019) 182–193.
- [53] D.N. Gray, G.P. Shulman, R.T. Conley, The mechanism of polybenzimidazole formation by condensation of aromatic tetramines and esters and the structure of the resulting polycondensates, J. Macromol. Sci. 1 (3) (1967) 395–411.
- [54] D. Aili, L.N. Cleemann, Q. Li, J.O. Jensen, E. Christensen, N.J. Bjerrum, Thermal curing of PBI membranes for high temperature PEM fuel cells, J. Mater. Chem. 22 (12) (2012) 5444–5453
- [55] H. Vogel, C.S. Marvel, Polybenzimidazoles, New thermally stable polymers, J. Polym. Sci. 50 (154) (1961) 511–539.
- [56] J.K. Gillham, Polymer structure: cross-linking of a polybenzimidazole, Science 139 (3554) (1963) 494–495.
- [57] G.P. Shulman, W. Lochte, Thermal degradation of polymers. IV. Poly-2,2'-(m-phenylene)-5,5'-bibenzimidazole, J. Macromol. Sci. 1 (3) (1967) 413–428.

- [58] S.R. Samms, S. Wasmus, R.F. Savinell, Thermal stability of proton conducting acid doped polybenzimidazole in simulated fuel cell environments, J. Electrochem. Soc. 143 (4) (1996) 1225–1232.
- [59] K.C. Khulbe, C.Y. Feng, T. Matsuura, Synthetic Polymeric Membranes -Characterization by Atomic Force Microscopy, Springer, Berlin, 2008.
- [60] M.M. Cordes, J.L. Walter, Infrared and Raman studies of heterocyclic compounds -II Infrared spectra and normal vibrations of benzimidazole and bis-(benzimidazolato)-metal complexes, Spectrochim. Acta, Part A 24 (9) (1968) 1421–1435
- [61] M. Cordes, J.L. Walter, Infrared and Raman spectra of heterocyclic compounds I the infrared studies and normal vibrations of imidazole, Spectrochim. Acta, Part A 24 (3) (1968) 237–252.
- [62] Y. Álvarez-Gallego, B. Ruffmann, V. Silva, H. Silva, A.E. Lozano, J.G. de la Campa, S.P. Nunes, J. de Abajo, Sulfonated polynaphthalimides with benzimidazole pendant groups, Polymer 49 (18) (2008) 3875–3883.
- [63] S.C. Kumbharkar, M.N. Islam, R.A. Potrekar, U.K. Kharul, Variation in acid moiety of polybenzimidazoles: investigation of physico-chemical properties towards their applicability as proton exchange and gas separation membrane materials, Polymer 50 (6) (2009) 1403–1413.
- [64] P. Musto, F.E. Karasz, W.J. MacKnight, Hydrogen bonding in polybenzimidazole/ polyimide systems: a Fourier-transform infra-red investigation using lowmolecular-weight monofunctional probes, Polymer 30 (6) (1989) 1012–1021.
- [65] D.M.W. Anderson, J.L. Duncan, F.J.C. Rossotti, The hydrogen bonding of imidazole in carbon tetrachloride solution, J. Chem. Soc. (0) (1961) 2165–2171.
- [66] P.A. Christensen, S.W.M. Jones, An in situ FTIR study of undoped PolyBenzoImadazole as a function of relative humidity, Polym. Degrad. Stabil. 105 (2014) 211–217.
- [67] P. Musto, P. La Manna, J.D. Moon, M. Galizia, B.D. Freeman, Infrared spectroscopy of polybenzimidazole in the dry and hydrate forms: a combined experimental and computational study, ACS Omega 3 (9) (2018) 11592–11607.
- [68] H. Zimmermann, Über den intermolekularen protonenübergang und über die zustände des protons in der wasserstoffbrückenbindung von imidazole, Z. Elektrochem., Ber. Bunsenges, Physik, Chem. 65 (10) (1961) 821–840.
- [69] R.P. Campion, G.J. Morgan, High pressure permeation and diffusion of gases in polymers of different structures, Plast., Rubber Compos. Process. Appl. 17 (1) (1992) 51–58.
- [70] Y. Wang, S.N. Rashkeev, J.R. Klaehn, C.J. Orme, E.S. Peterson, Interaction of gas molecules with crystalline polymer separation membranes: atomic-scale modeling and first-principles calculations, J. Membr. Sci. 384 (1–2) (2011) 176–183.
- [71] T.D. Dang, L.S. Tan, F.E. Arnold, Benzimidazole pendent rigid-rod benzobisthiazole polymers, Polym. Preprint. 31 (1990) 451–452.
- [72] D.W. Tomlin, A.V. Fratini, M. Hunsaker, W. Wade Adams, The role of hydrogen bonding in rigid-rod polymers: the crystal structure of a polybenzobisimidazole model compound, Polymer 41 (25) (2000) 9003–9010.
- [73] L.M. Robeson, The upper bound revisited, J. Membr. Sci. 320 (2008) 390–400.
- [74] B.W. Rowe, L.M. Robeson, B.D. Freeman, D.R. Paul, Influence of temperature on the upper bound: theoretical considerations and comparison with experimental results. J. Membr. Sci. 360 (1–2) (2010) 58–69.
- [75] B.W. Rowe, L.M. Robeson, B.D. Freeman, D.R. Paul, Corrigendum to "Influence of temperature on the upper bound: theoretical considerations and comparison with experimental results", J. Membr. Sci. 366 (1–2) (2011) 436 [J. Membr. Sci. 360 (2010) 58–69].
- [76] J. Crank, The Mathematics of Diffusion, 2 ed., 1975. Oxford, England, UK.
- [77] R.E. Kesting, A.K. Fritzsche, Polymeric Gas Separation Membranes, Wiley-Interscience, USA, 1993.
- [78] J.E. Lundstrom, A statistical model for diffusion in polymers, Trans. NY Acad. Sci. 35 (2 Series II) (1973) 95–111.
- [79] K.D. Ziegel, F.R. Eirich, Isotope effect in gas transport. I. Measurement of the free volume element in four polymers above the glass transition temperature, J. Polym. Sci. A-2 Polym. Phys. 8 (11) (1970) 2015–2027.